Bull Math Biol (2017) 79:1923–1978
DOI 10.1007/s11538-017-0314-1

Society for Mathematical Biology

ORIGINAL ARTICLE

Application of Quasi-Steady-State Methods to Nonlinear Models of Intracellular Transport by Molecular Motors

Cole Zmurchok[1] · **Tim Small**[1] · **Michael J. Ward**[1] · **Leah Edelstein-Keshet**[1]

Received: 6 April 2017 / Accepted: 22 June 2017 / Published online: 13 July 2017

Abstract Molecular motors such as kinesin and dynein are responsible for transporting material along microtubule networks in cells. In many contexts, motor dynamics can be modelled by a system of reaction–advection–diffusion partial differential equations (PDEs). Recently, quasi-steady-state (QSS) methods have been applied to models with linear reactions to approximate the behaviour of the full PDE system. Here, we extend this QSS reduction methodology to certain nonlinear reaction models. The QSS method relies on the assumption that the nonlinear binding and unbinding interactions of the cellular motors occur on a faster timescale than the spatial diffusion and advection processes. The full system dynamics are shown to be well approximated by the dynamics on the slow manifold. The slow manifold is parametrized by a single scalar quantity that satisfies a scalar nonlinear PDE, called the QSS PDE. We apply the QSS method to several specific nonlinear models for the binding and unbinding of molecular motors, and we use the resulting approximations to draw conclusions regarding the parameter dependence of the spatial distribution of motors for these models.

Keywords Quasi-steady-state · Molecular motors · Intracellular transport · Nonlinear kinetics

1 Introduction

Diffusion is a fast transport mechanism on the length scale of a typical cell, a few tens of micrometres. However, some specialized cells, including neurons, are up to 1 m in

Michael J. Ward and Leah Edelstein-Keshet are co-supervising authors.

✉ Cole Zmurchok
zmurchok@math.ubc.ca

[1] Department of Mathematics, University of British Columbia, Vancouver V6T 1Z2, Canada

length. This length scale imposes dramatic constraints on the transport of structural, metabolic, and signalling components from the neuronal cell body (the soma) to the ends of dendrites or axons. Molecular diffusion is extremely inefficient at such length scales. Hence, cells have evolved active transport mechanisms consisting of molecular motors that bind to microtubule tracks and convey cargo packaged in vesicles across the cell (Chowdhury et al. 2005).

Microtubules (MTs) are asymmetric, having distinct "plus" and "minus" ends. The two major types of molecular motors, kinesin and dynein, walk processively on microtubules in opposite directions: kinesin walks towards the plus ends, while dynein walks towards the minus ends of MTs. Both motors exist in several states, including unbound, cytoplasmic forms (Blasius et al. 2013), and MT-bound (the focus of our paper) as well as bound singly or in groups to cargo (not discussed here). The overall traffic of motors across the cell depends on the polarity and configuration of MTs, the rates of binding to and unbinding from MTs, and the motor speeds while bound. Transport also depends on molecular diffusion in the cytosol. Some, but not all of these factors can be experimentally observed in neurons, or in simpler model systems such as filamentous fungi, where genetic and in vitro manipulations are far easier to conduct.

One convenient experimental system is *Ustilago maydis*, a fungus whose long filamentous hyphae contain MTs of mixed polarity (Fink and Steinberg 2006; Schuster et al. 2011a, b; Steinberg 2011; Steinberg et al. 2001). Microtubules of mixed polarity also occur in the proximal regions of neuronal dendrites (Baas et al. 1988; Burton 1988; Stone et al. 2008). In these systems, particularly in the fungal hyphae, motors have been observed to move bidirectionally: first towards one cell end and then towards the opposite end. This observation can be explained in one of two ways. Either multiple motors (dynein and kinesin) bound to the same cargo can "take turns" pulling the load, or else a single motor, by detaching and binding to a MT of opposite polarity, would then change its direction of motion. Here we consider the latter scenario.

One question that has intrigued modellers is how to bridge between the rates and events at the molecular level (binding, unbinding, and motor speeds) and the overall cargo distribution and effective transport speed at the cellular level (Shubeita 2012). This has motivated the development of a number of mathematical models at various levels of detail. A number of efforts have dealt with the tug-of-war or teamwork of several motors attached to a single cargo (Bhat and Gopalakrishnan 2012; Hendricks et al. 2010; Klumpp and Lipowsky 2005; Mallik et al. 2013; Müller et al. 2008). In many cases, such models mandate stochastic and computational approaches, that consider multiple states (n, m motors of distinct types attached to a cargo, etc.). Other approaches simplify the problem to consider only a few states and formulate transport equations (Smith and Simmons 2001) or derive such PDEs from a master-equation approach to the stochastic motor behaviour. Examples of such approaches include (1) an analysis and mean-field approximation of the dynamics of the totally asymmetric simple exclusion process with Langmuir kinetics (Parmeggiani et al. 2004), (2) a study of the spontaneous formation of traffic "jams" resulting from transport on two parallel lanes (two parallel microtubule tracks) (Reichenbach et al. 2007), and (3) the incorporation of a kinetic model for motor stepping dynamics and a study of the resulting effects on collective transport (Ciandrini et al. 2014). We follow the novel and elegant

linear theory developed by Bressloff and Newby (2013) and Newby and Bressloff (2010b) for important insights into motor function by deriving a quasi-steady-state (QSS) Fokker–Planck equation from which the parameter dependence of the motor distribution can be predicted, and by connecting molecular events to overall effective diffusion and transport velocity. Although this linear theory is based on simplifications and assumptions (e.g. that the binding/unbinding kinetics are fast on the timescale of transport across the cell), it provides a useful way to gain insight into the role of various parameters in determining the overall functionality of the transport system.

In recent work, Gou et al. (2014) used the PDE approach to model the transport of early endosomes (cargo transported by kinesin and dynein) inside *Ustilago maydis*, arriving at good agreement with experimental observations, and posing several hypotheses for further experimental studies. A follow-up paper (Dauvergne and Edelstein-Keshet 2015) applied the methods of Bressloff and Newby (2013) and Newby and Bressloff (2010b) to the examples motivated by Gou et al. (2014). In both these recent works, the models included microtubules of mixed polarity, with and without a bias towards one end of the (1-D) cell, and linear rates of binding and unbinding from the MT. Results in Dauvergne and Edelstein-Keshet (2015), for example, demonstrate that the effective velocity of transport is the average of motor velocities, weighted by the fraction of time spent in a given state, whereas the effective diffusivity is similarly such an average, but includes an additional term that represents a variance in velocities of motor in different states.

Linearity of the binding rates presumes that there is no interaction between groups of motors and that binding sites are ample and unlimited. But in many biological situations, such assumptions are unwarranted. Cases in which complicated, possibly nonlinear, features have been observed are in molecular motor traffic jams (Leduc et al. 2012) and exclusion of one motor by others (Schneider et al. 2006). Another case is the effect of microtubule-associated proteins (MAPS) such as tau that modulates the ability of motors to bind to MTs or to stay bound (Dixit et al. 2008; McVicker et al. 2011). MTs can also have various post-translational modifications that affect the availability or affinity of binding sites to motors [for example, kinesin-1 binds with higher affinity to MTs that have been modified by acetylation (Reed et al. 2006)]. Considering such effects leads to models in which the binding or unbinding is nonlinear and saturating, or to models that mass-action products terms that represent motor interactions. The effect of spatially varying parameters resulting from non-homogeneous MT polarity, ATP gradients, and MAPS has been investigated in the context of intracellular transport in neuronal cells using quasi-steady-state methodology (Newby and Bressloff 2010a), yet the effect of nonlinear kinetic terms has been largely unexplored analytically. The need to generalize previous analysis to include models with such nonlinearities motivates our approach in this paper.

Our main mathematical focus, discussed in detail in Sect. 3, is to extend the quasi-steady-state (QSS) reduction method introduced in Newby and Bressloff (2010b) for reaction–advection–diffusion systems with linear reaction kinetics to a class of problems where the kinetics are nonlinear, but where a conservation condition is satisfied. The latter represents the fact that motors transit between states, but are conserved overall. The QSS method relies on the assumption that the nonlinear kinetics occur on a faster timescale than the diffusion and advection processes. Owing to the conservation

condition, in this limit of fast reaction kinetics, a one-parameter family of quasi-steady-state solutions is obtained from the equilibrium state of the kinetics. When there are no eigenvalues of the linearization of the kinetics along this one-parameter family that lie in the unstable right half-plane, this quasi-steady-state solution is referred to as a slow solution manifold for the full reaction–advection–diffusion system. When this condition on the Jacobian of the nonlinear kinetics is satisfied, we use an asymptotic expansion together with a Fredholm alternative condition to derive a single scalar quasi-steady-state PDE, which effectively parameterizes the slow solution manifold.

In Sect. 4 we then apply the asymptotic formalism of Sect. 3 to analyse three specific three-component nonlinear systems for the binding and unbinding of molecular motors. These three specific models are formulated in Sect. 2 and consist of (1) A model for a single motor ("kinesin") transiting between motion along right-pointing MTs, diffusion in the cytosol, and motion along left-pointing MTs (with transitions only through the cytoplasmic pool), (2) a model for kinesin–dynein-cargo complexes moving left or right along MTs or diffusing in the cytosol (interactions on a MT assumed to lead to motor swaps that also change the direction of motion), and (3) a model for motors ("unconventional myosin") whose encounters on an actin filament lead to stalling. In all three cases, motors exchange between cytosolic diffusible states and states bound to a track (MT or actin). Nonlinearity stems from saturated binding kinetics in (1), mass-action motor interactions leading to swaps in (2), and to stalling in (3).

Overall, our QSS PDE is used to analyse the behaviour of steady-state solutions of the full reaction–advection–diffusion system as parameters are varied, and the results are then interpreted biologically. The main conclusion is that in all three cases studied, the resulting QSS PDE is a conservation law for the total density within the cell, with effective velocity and effective diffusion that depend nonlinearly on the model parameters and motor density. We make predictions about the full model behaviour through the analytical insight gained through the QSS reduction, and the effective velocity and effective diffusion functions. To verify our QSS method and analysis, we use numerical simulations to study the steady-state and time-dependent behaviour of both the full models and the QSS PDE. In particular, we use the MATLAB function `pdepe` for time-dependent numerical simulations and also recast the steady-state QSS PDE as a initial boundary value problem, which is amenable to numerical solution with a shooting method ("Appendix C").

In the kinesin motor model, the nonlinear interactions depend on the density of cytosolic motors. The QSS PDE describes the bulk motor distribution through effective velocity and diffusion coefficients. These effective coefficients are related to the original velocity and diffusion coefficients weighted by the time spent in the directed-movement and random-movement states. Moreover, the polarity distribution of MTs affects the bulk motor distribution by changing the sign of the velocity, which can bias the distribution of motors to the right or left end of the cell.

Unlike the kinesin motor model, the nonlinear kinetics in the kinesin–dynein motor complex model arise due to a mass-action law which describes the rate at which motor complexes turn in response to motor complexes heading in the other direction. In this case, the resulting QSS PDE is again a conservation law for the total amount of motor complexes, with the advection speed dependent on the motor complex speed,

the turning rate, and which motors in the complex are active. In addition to these parameters, the resulting diffusion coefficient is dependent on the binding affinity of the motor complex to MTs. We find that a sufficiently high turning rate can reverse the distribution of motor complexes from one end of the cell to the other, even if the probability of moving to one end of the cell is high.

In the myosin motor model, reaction kinetics that model the transition to the stalled state result in two different QSS PDEs. In the first case, the motors equilibrate between freely diffusing and walking on MT, without any motors in the stalled state. In the second case, there are some motors in the stalled state. In the first case, the QSS PDE is linear, with effective diffusion coefficient and effective velocity mediated by the binding rate of myosin motors. We find that the asymptotic solution compares favourably with full numerical simulations of the myosin model. In the second case, the resulting QSS PDE is nonlinear, but is a conservation law for the total density of myosin motor. The effective transport rate depends on the density of stalled motors, the velocity of stalled motors due to actin treadmilling, and the stalling rate. The effective rate of diffusion depends on all model parameters except for the velocity of stalled motors due to treadmilling. The second QSS is only valid for a range of parameter space and stalled motor density. Outside of this range, the QSS PDE is ill-posed. A further novel feature of the myosin model is that the full system always converges to the first QSS, where there are no stalled motors. Through a boundary layer analysis ("Appendix D"), we determine that this results from the boundary conditions. We suggest and study an alternate myosin model which has the same QSS approximations but, depending on initial conditions, can realize either state.

The paper concludes with a brief discussion in Sect. 5.

2 Model Development

We model the cell as a 1-D tube of length L_0, with its left end at $x = 0$. The densities of motors are described as number per unit cell length, with the cross-sectional area of the cell assumed to be constant. Molecular motors exist in any number, n, of possible states within the cell, with $p_i(x, t)$ denoting the density of motors in state i.

We use a reaction–advection–diffusion system to describe the evolution of the vector density $\mathbf{p} \equiv (p_1, \ldots, p_n)^T$ of motors as

$$\frac{\partial \mathbf{p}}{\partial t} = \mathbf{M}(\mathbf{p}) + \mathbf{f}(\mathbf{p}), \tag{1}$$

where $\mathbf{f} \equiv (f_1, \ldots, f_n)^T$ describes the state transition rates and $\mathbf{M}$ is a linear matrix differential operator characterizing the advection and diffusion of motors in each state. We assume that the ends of the cells are closed, and impose an overall zero-flux condition at the cell ends. In addition, we assume that the motors are exchanged between states in such a way that there is no net loss or gain of motors, i.e. that

$$\sum_{i=1}^{n} f_i = 0. \tag{2}$$

These two assumptions result in conservation of the total density of molecular motor in the cell.

Our goal is to develop a theoretical framework to analyse models of the form (1) where the reaction term $\mathbf{f}$ is nonlinear and occurs on a timescale that is fast relative to the timescale of the advection and diffusion processes. This theory is then applied to three specific nonlinear binding mechanisms. In Sects. 2.1 and 4.1 we consider a nonlinear kinesin model; in Sects. 2.2 and 4.2 we consider a nonlinear kinesin–dynein model; while in Sects. 2.3 and 4.3 we consider a nonlinear myosin model. Our analysis extends the previous analysis for linear binding models developed in Bressloff and Newby (2013), Dauvergne and Edelstein-Keshet (2015) and Newby and Bressloff (2010b) to allow for nonlinear binding mechanisms.

2.1 Kinesin Model

In hyphae of the fungus, *Ustilago maydis*, for example, kinesin motors walk along microtubules within the cell or diffuse freely in the cytosol (Dauvergne and Edelstein-Keshet 2015; Gou et al. 2014; Schuster et al. 2011a, b; Steinberg 2011). The density $p^{\mathrm{R}}(x,t)$ [respectively, $p^{\mathrm{L}}(x,t)$] represents the population of kinesin bound to right-polarized (respectively, left-polarized) MTs walking towards the end of the cell at $x = L_0$ (respectively, $x = 0$). The population of freely diffusing cytosolic kinesin is modelled by the density $p^{\mathrm{U}}(x,t)$ (U for unbound). Inside this 1-D domain, $0 \leq x \leq L_0$, the microtubule distribution is described by $0 \leq P(x) \leq 1$, which represents the fraction of MTs pointing to the right at a point x. Since kinesin always walks towards a MT plus end, it can reverse its direction of motion only by unbinding from a given MT and rebinding to a MT of opposite polarity. For this reason, we can assume that, in this model, motor transitions occur only through the cytosolic state. We describe the spatiotemporal evolution of the kinesin densities by the transport equations (see the schematic diagram in Fig. 1):

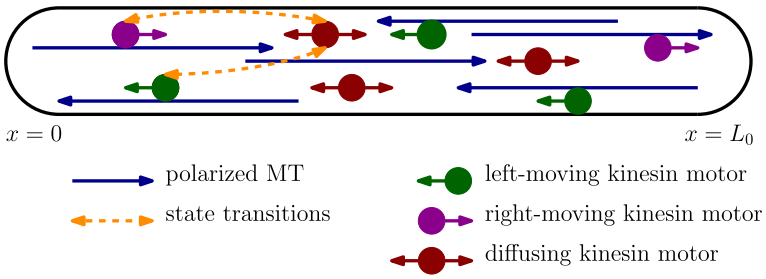

Fig. 1 A schematic diagram of kinesin-based intracellular transport in a 1-D cell of length L_0. Kinesin motors can bind to polarized microtubules (MTs, *blue arrows*) and move to the right (*purple circles* with *right-pointing arrows*) or to the left (*green circles* with *left-pointing arrows*). While unbound, kinesin motors are free to diffuse in the cell's cytoplasm (*red circles* with *right-* and *left-pointing arrows*). State transitions (*orange dashed arrows*) occur through the freely diffusing cytosolic state (Color figure online)

$$\frac{\partial p^{\mathrm{R}}}{\partial t} = -v\frac{\partial p^{\mathrm{R}}}{\partial x} + Pk_{\mathrm{b}}g(p^{\mathrm{U}}) - k_{\mathrm{u}}p^{\mathrm{R}}, \tag{3a}$$

$$\frac{\partial p^{\mathrm{L}}}{\partial t} = v\frac{\partial p^{\mathrm{L}}}{\partial x} + (1-P)k_{\mathrm{b}}g(p^{\mathrm{U}}) - k_{\mathrm{u}}p^{\mathrm{L}}, \tag{3b}$$

$$\frac{\partial p^{\mathrm{U}}}{\partial t} = D_0\frac{\partial^2 p^{\mathrm{U}}}{\partial x^2} - k_{\mathrm{b}}g(p^{\mathrm{U}}) + k_{\mathrm{u}}p^{\mathrm{R}} + k_{\mathrm{u}}p^{\mathrm{L}}. \tag{3c}$$

In Eqs. (3), bound kinesin moves to the right or to the left with velocity v, and D_0 is the diffusion coefficient for cytosolic kinesin. The unbinding rate is k_{u}, while the binding rates for kinesin binding to right-polarized and left-polarized MTs are $k_{\mathrm{b}}Pg(p^{\mathrm{U}})$ and $k_{\mathrm{b}}(1-P)g(p^{\mathrm{U}})$, respectively. Here, $P = P(x)$ is the fraction of MTs polarized towards the right in the cell. Here we have assumed a constant density of MTs across the cell (absorbed into the constant k_{b}). We discuss a generalization to non-uniform MT density $m(x)$ in "Appendix A.1". The function $g(p^{\mathrm{U}})$, possibly nonlinear, describes how other processes such as competition for binding sites or binding cooperativity are modelled. For instance, saturated binding due to a limited number of binding sites could be depicted by a term of the form

$$g(p^{\mathrm{U}}) = g_{\mathrm{m}}\frac{p^{\mathrm{U}}}{K + p^{\mathrm{U}}}, \tag{4}$$

for some parameters $K > 0$ and $g_{\mathrm{m}} > 0$ [forms such as (4) are obtained by assumptions typical of Michaelis–Menten kinetics]. Conservation of the kinesin motors within the cell implies that zero-flux boundary conditions are required to model the impermeable cell ends:

$$\left(vp^{\mathrm{R}} - vp^{\mathrm{L}} - D_0\frac{\partial p^{\mathrm{U}}}{\partial x}\right)\Bigg|_{x=0,L_0} = 0. \tag{5}$$

The two additional boundary conditions are that there is no right-moving kinesin at the left endpoint of the cell and no left-moving kinesin at the right endpoint. These boundary conditions result from the fact that to create a flux of right-moving kinesin at a given point, there had to be a kinesin bound to a MT to the left of that point—which is impossible at $x = 0$, the leftmost point in the cell. A similar argument at the rightmost point in the cell establishes the right endpoint. Thus, we require that the following two Dirichlet conditions hold:

$$vp^{\mathrm{R}}(0) = 0 \quad \text{and} \quad vp^{\mathrm{L}}(L_0) = 0. \tag{6}$$

2.2 Kinesin–Dynein Model

The three-state kinesin model, formulated in Sect. 2.1, is a simplification of intracellular cargo transport. Cargo in fungal hyphae is typically bound to one dynein and four or five kinesin motors at a time (Schuster et al. 2011a). In this case, the entire kinesin–dynein-cargo complex may be transported towards or away from the cell tip,

depending on which motors are actively involved in the transport process and the polarity of the MTs to which they are bound. We now describe a simple model for the organization and transport of cargo bound to a kinesin–dynein motor complex.

The populations of kinesin–dynein-cargo complexes are divided into right-moving, left-moving, and freely diffusing subclasses, regardless of the molecular motors active in the transport process. In the three-state kinesin model, the nonlinearities were restricted to binding and unbinding interactions. To explore the effect of nonlinear interactions between motors in distinct subclasses, we now consider linear binding and unbinding interactions, but allow for a nonlinear interaction term between the right- and left-moving species when they are in proximity on a MT. We seek to apply our QSS theory to a model of this type, as Yochelis and Gov (2016) have recently used a model with a similar nonlinear interaction to describe the spatial organization and dynamics of unconventional myosin motors in actin-based protrusions.

The population of right-moving (respectively, left-moving) motor complexes walking towards the end of the cell at $x = L_0$ (respectively, $x = 0$) is described by density $p^{\mathrm{R}}(x,t)$ (respectively, $p^{\mathrm{L}}(x,t)$). The population of freely diffusing cytosolic motor complexes is described by density $p^{\mathrm{U}}(x,t)$. Here we define a "binding bias" function, Q, that represents the probability that when a free motor complex binds to a MT, it becomes a right-moving motor complex. Then (assuming no stalled states on the MT) the probability of becoming a left-moving motor complex, upon binding to a MT, is $(1-Q)$. Since kinesin walks towards the plus ends, while dynein walks towards the minus ends, of MTs, the function $Q(x)$ actually comprises several biological quantities, including local MT polarity, ratio of kinesin to dynein molecules in a complex, as well as respective affinities to MTs of these two motors. In "Appendix A.2" we discuss how this simplification by a single function can be related to such biological factors. An important distinction between this and the previous model is that now direction switching can take place on a MT and does not require unbinding into the cytosol.

The above simplification allows for the detailed study of a nonlinear interaction between right- and left-moving populations. We assume that when a right-moving complex meets a left-moving complex, the right-moving complex changes direction with rate k_{rl}. Similarly, when a left-moving complex meets a right-moving complex, the right-moving complex changes direction with rate k_{lr}. (These direction changes are due to a swap between a motor that is actively walking, e.g. dynein, and its passive partner motor kinesin, or vice versa, in the given complex.) Freely diffusing motor complex binds to MTs at rate k_{b} and diffuses in the cytosol with diffusion coefficient D_0. Bound motor complexes can move to the right (or left) with velocity v_{r} (or v_{l}), or they can unbind from MTs with rate k_{u}. These assumptions lead to the following reaction–advection–diffusion system on $0 \le x \le L_0$ (see the schematic diagram in Fig. 2):

$$\frac{\partial p^{\mathrm{R}}}{\partial t} = -v_{\mathrm{r}}\frac{\partial p^{\mathrm{R}}}{\partial x} + k_{\mathrm{b}}Qp^{\mathrm{U}} - k_{\mathrm{u}}p^{\mathrm{R}} - k_{\mathrm{rl}}p^{\mathrm{R}}p^{\mathrm{L}} + k_{\mathrm{lr}}p^{\mathrm{L}}p^{\mathrm{R}}, \tag{7a}$$

$$\frac{\partial p^{\mathrm{L}}}{\partial t} = v_{\mathrm{l}}\frac{\partial p^{\mathrm{L}}}{\partial x} + k_{\mathrm{b}}(1-Q)p^{\mathrm{U}} - k_{\mathrm{u}}p^{\mathrm{L}} + k_{\mathrm{rl}}p^{\mathrm{R}}p^{\mathrm{L}} - k_{\mathrm{lr}}p^{\mathrm{L}}p^{\mathrm{R}}, \tag{7b}$$

$$\frac{\partial p^{\mathrm{U}}}{\partial t} = D_0\frac{\partial^2 p^{\mathrm{U}}}{\partial x^2} - k_{\mathrm{b}}p^{\mathrm{U}} + k_{\mathrm{u}}(p^{\mathrm{R}} + p^{\mathrm{L}}). \tag{7c}$$

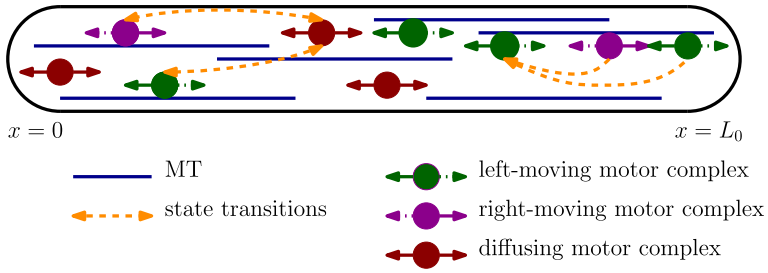

Fig. 2 As in Fig. 1 but for the kinesin–dynein motor complexes. *Colour code* as before for MT, and for left- or right-moving or diffusing complexes. A new feature is that state transitions can also occur through the collision of a left- and right-moving motor complex (*orange dashed arrows*, right) (Color figure online)

If we define $k_c \equiv k_{rl} - k_{lr}$, this model can be written as

$$\frac{\partial p^R}{\partial t} = -v_r \frac{\partial p^R}{\partial x} + k_b Q p^U - k_u p^R - k_c p^R p^L, \tag{8a}$$

$$\frac{\partial p^L}{\partial t} = v_l \frac{\partial p^L}{\partial x} + k_b (1 - Q) p^U - k_u p^L + k_c p^R p^L, \tag{8b}$$

$$\frac{\partial p^U}{\partial t} = D_0 \frac{\partial^2 p^U}{\partial x^2} - k_b p^U + k_u (p^R + p^L). \tag{8c}$$

Conservation of the motor complexes within the cell implies that zero-flux boundary conditions are required to model the impermeable cell ends:

$$\left(v_r p^R - v_l p^L - D_0 \frac{\partial p^U}{\partial x} \right) \Bigg|_{x=0, L_0} = 0. \tag{9}$$

The remaining two boundary conditions are that

$$v_r p^R(0) = 0 \quad \text{and} \quad v_l p^L(L_0) = 0. \tag{10}$$

2.3 Myosin Model

Like kinesin and dynein motors, unconventional myosin motors are also responsible for intracellular transport in actin-based cellular protrusions, such as filopodia and stereocilia (Nambiar et al. 2010). Filopodia are long, thin cellular protrusions with actin filaments at their core. These structures are involved in cell motility, adhesion, and communication (Mattila and Lappalainen 2008). Stereocilia are highly organized protrusions on hair-cells of the inner ear, responsible for hearing (Schwander et al. 2010). The actin-based filamentous scaffold that supports these protrusions is known to undergo turnover, which is maintained by the delivery of new actin monomer subunits to the distal ends of the protrusions, and the disassembly of the actin bundle at its base (Rzadzinska et al. 2004). (The apparent motion of the actin filament bundle

due to continual assembly and disassembly at opposite ends is called treadmilling.) The transport of those monomers and other materials is facilitated by unconventional myosin motors (Nambiar et al. 2010). In Yochelis and Gov (2016) and Yochelis et al. (2015), a reaction–advection–diffusion model was employed to describe the self-organization of waves and pulse trains in myosin motor distribution along cell protrusions. Inspired by their model, we consider a simplified system with the same nonlinear cross-species interaction term to demonstrate that the QSS method can be applied.

We consider three populations of myosin motors: bound (p^{B}), walking (p^{W}), and unbound or freely diffusing (p^{U}) in a 1-D geometry. We suppose that the base of the protrusion of length L_0 is at $x = 0$, but assume that the protrusion is self-contained and impose zero total flux boundary conditions at both ends. Adapted from Yochelis and Gov (2016) and Yochelis et al. (2015), the myosin dynamics are described by the following set of reaction–advection–diffusion equations on $0 \le x \le L_0$:

$$\frac{\partial p^{\mathrm{W}}}{\partial t} = -v_{\mathrm{w}}\frac{\partial p^{\mathrm{W}}}{\partial x} - \hat{k}_{\mathrm{bw}}\left(p^{\mathrm{B}}\right)^2 p^{\mathrm{W}} + \hat{k}_{\mathrm{b}}p^{\mathrm{U}} - k_{\mathrm{u}}p^{\mathrm{W}}, \tag{11a}$$

$$\frac{\partial p^{\mathrm{B}}}{\partial t} = v_{\mathrm{b}}\frac{\partial p^{\mathrm{B}}}{\partial x} + \hat{k}_{\mathrm{bw}}\left(p^{\mathrm{B}}\right)^2 p^{\mathrm{W}} - k_{\mathrm{u}}p^{\mathrm{B}}, \tag{11b}$$

$$\frac{\partial p^{\mathrm{U}}}{\partial t} = D_{\mathrm{f}}\frac{\partial^2 p^{\mathrm{U}}}{\partial x^2} - \hat{k}_{\mathrm{b}}p^{\mathrm{U}} + k_{\mathrm{u}}(p^{\mathrm{B}} + p^{\mathrm{W}}). \tag{11c}$$

Due to actin treadmilling, bound (stalled) motors are effectively transported towards the base of the actin bundle with the treadmilling velocity v_{b}. Bound motors unbind with rate k_{u} and walking motors can become bound if they encounter a sufficiently high density of bound motors ($\hat{k}_{\mathrm{bw}}\left(p^{\mathrm{B}}\right)^2 p^{\mathrm{W}}$). Walking motors, on the other hand, move to the distal end of the cell protrusion with velocity v_{w}. Walking motors may also unbind to become freely diffusing motors. The freely diffusing motors have diffusion coefficient D_{f} and can reattach to an actin filament and transition to a walking motor with rate $\hat{k}_{\mathrm{b}}$.

We assume that the total flux of myosin is zero at either end of the protrusion, which gives the boundary condition

$$\left(v_{\mathrm{w}}p^{\mathrm{W}} - v_{\mathrm{b}}p^{\mathrm{B}} - D_{\mathrm{f}}\frac{\partial p^{\mathrm{U}}}{\partial x}\right)\Bigg|_{x=0,L_0} = 0. \tag{12}$$

As before, we also have two additional boundary conditions

$$v_{\mathrm{w}}p^{\mathrm{W}}(0) = 0 \quad \text{and} \quad v_{\mathrm{b}}p^{\mathrm{B}}(L_0) = 0, \tag{13}$$

which ensures that there is no right-moving and left-moving myosin at the left and right endpoints, respectively.

3 Quasi-Steady-State Reduction

The quasi-steady-state (QSS) reduction method, developed in Bressloff and Newby (2013) for the case where the vector $\mathbf{f}$ of state transitions is linear, will be extended to allow for nonlinear $\mathbf{f}$. In this asymptotic approach, the key assumption is that the timescale associated with transitions between states, represented by binding and unbinding mechanisms, is short relative to the time it takes for motors to move across the cell. This introduces a small parameter $\varepsilon \approx v/(L_0 k)$, where v is the motor velocity, L_0 is the cell length, and k is a typical transition rate.

Using the QSS approximation, we aim to reduce the system of transport equations to a scalar nonlinear PDE describing the dynamics of the system for small ε. To this end, we rescale space and time so that the length of the cell is $L_0 = 1$ and so that one of the motor subpopulations moves with speed $v_i = 1$. We scale distance by the cell length; we scale time by the time it takes for a walking motor to move across the cell. That is, we introduce

$$x^\star = \frac{x}{L_0}, \qquad t^\star = \frac{t v_i}{L_0}. \tag{14}$$

Under this scaling, and with the assumption that the timescale associated with transitions between states is short, we can write the system (1), upon dropping the starred coordinates, as

$$\frac{\partial \mathbf{p}}{\partial t} = \mathbf{M}(\mathbf{p}) + \frac{1}{\varepsilon}\mathbf{f}(\mathbf{p}), \tag{15}$$

where $\mathbf{f}(\mathbf{p})$ represents the $\mathscr{O}(1)$ nonlinear motor state transition kinetics. Here $\mathbf{M}$ is the linear $n \times n$ matrix differential operator in the rescaled coordinates, with zero off-diagonal entries, so that $\mathbf{M}_{ij} = 0$ for $i \neq j$, and diagonal entries $\mathbf{M}_{ii} = -v_i \partial/\partial x + D_i \partial^2/\partial x^2$ for $i = 1, \ldots, n$, with v_i possibly not all unity if the right- and left-moving motors have different speeds. Details of the scaling leading to (15) for our three specific systems are given in "Appendix A.2".

The QSS reduction method exploits the assumed small parameter ε in (15). On a short timescale, where $t = \mathscr{O}(\varepsilon)$ so that $\tau = t/\varepsilon$, (15) yields

$$\frac{\partial \mathbf{p}}{\partial \tau} = \mathbf{f}(\mathbf{p}) + \mathscr{O}(\varepsilon). \tag{16}$$

Ignoring $\mathscr{O}(\varepsilon)$ terms, this nonlinear ODE system describes the well-mixed dynamics to leading-order on a short timescale. We define the quasi-steady-state, $\mathbf{p}^0$, of (15) to be the steady-state of this well-mixed system, i.e. $\mathbf{f}(\mathbf{p}^0) = \mathbf{0}$. For a general nonlinear function $\mathbf{f}$, a solution to $\mathbf{f}(\mathbf{p}^0) = \mathbf{0}$ is not guaranteed. We will restrict attention to $\mathbf{f}$ such that (16) has a steady-state solution. However, due to the conservation (2) of motors within the cell, to solve $f_1(\mathbf{p}^0) = \cdots = f_n(\mathbf{p}^0) = 0$, it suffices to solve the under-determined algebraic system $f_1(\mathbf{p}^0) = \cdots = f_{n-1}(\mathbf{p}^0) = 0$. From this, we automatically find $f_n(\mathbf{p}^0) = 0$. As such, generically, when a steady-state exists it can be written parametrically as $\mathbf{p}^0 = \mathbf{p}^0(\alpha)$ in terms of some scalar quantity $\alpha = \alpha(x, t)$.

As there may be more than one solution to $\mathbf{f}(\mathbf{p}^0) = \mathbf{0}$, in order to ensure that we have found the steady-state to which the system (15) can converge, we need to introduce the following concept of the *slow manifold*:

Definition 3.1 Let $\mathbf{p}^0(\alpha)$ be a solution to $f_1 = \cdots = f_{n-1} = 0$. Then $\mathbf{p}^0(\alpha)$ is a slow manifold of (15) provided that the Jacobian matrix

$$\mathbf{J} = \mathbf{J}(\alpha) \equiv \left.\begin{pmatrix} f_{1p_1} & \cdots & f_{1p_n} \\ \vdots & \ddots & \vdots \\ f_{np_1} & \cdots & f_{np_n} \end{pmatrix}\right|_{\mathbf{p}=\mathbf{p}^0(\alpha)}, \tag{17}$$

has all eigenvalues satisfying $\Re(\lambda) \leq 0$ for all α on the range of definition. Moreover, $\lambda = 0$ is always an eigenvalue of $\mathbf{J}$ for any α, i.e. $\mathbf{J}\phi = 0$ for some $\phi \neq \mathbf{0}$.

To motivate the need for such a criterion, we introduce the new timescale $\tau = t/\varepsilon$, so that (15) reduces to leading-order to

$$\frac{\partial \mathbf{p}}{\partial \tau} = \mathbf{f}(\mathbf{p}). \tag{18}$$

In order for the ODE dynamics (18) to have the limiting behaviour

$$\lim_{\tau \to \infty} \mathbf{p}(\tau) = \mathbf{p}^0(\alpha_0), \tag{19}$$

at least for initial conditions near the slow manifold $\mathbf{p}^0$, where α_0 is determined by the initial condition, we must ensure that the eigenvalues of the Jacobian $\mathbf{J}(\alpha)$ satisfy $\Re(\lambda) \leq 0$ for all values of α. By differentiating

$$\mathbf{f}(\mathbf{p}^0(\alpha)) = \mathbf{0},$$

with respect to α, we readily observe that $\mathbf{J}$ must always have a zero eigenvalue, i.e. that

$$\mathbf{J}\phi = 0, \qquad \text{where} \qquad \phi = \frac{d\mathbf{p}^0}{d\alpha}(\alpha). \tag{20}$$

We must therefore ensure that the remaining eigenvalues of $\mathbf{J}(\alpha)$ satisfy $\mathrm{Re}(\lambda) < 0$. This leads to our key assumption on the nonlinearity $\mathbf{f}$.

Assumption 3.2 We assume that the vector $\mathbf{f}$ of state transitions is such that there is exactly one solution branch $\mathbf{p}^0(\alpha)$ to $\mathbf{f} = \mathbf{0}$ for which the condition on the Jacobian $\mathbf{J}$ in Definition 3.1 holds. Further, we assume that the zero eigenvalue of $\mathbf{J}$ has multiplicity one for any α on its range of definition.

With this assumption, we now show how to derive a nonlinear PDE for the evolution of $\alpha(x, t)$ in the quasi-steady-state $\mathbf{p}^0(\alpha)$. To do so, we expand $\mathbf{p}$ as a series in ε about the quasi-steady-state as

$$\mathbf{p} = \mathbf{p}^0(\alpha) + \varepsilon \mathbf{p}^1 + \cdots. \tag{21}$$

Upon substituting this expansion into (15) we obtain that

$$\mathbf{p}_t^0 + \varepsilon \mathbf{p}_t^1 + \cdots = \frac{1}{\varepsilon}\mathbf{f}(\mathbf{p}^0 + \varepsilon \mathbf{p}^1) + M\mathbf{p}^0 + \varepsilon M\mathbf{p}^1 + \cdots . \tag{22}$$

By using a Taylor expansion for the nonlinear term, together with the fact that $\mathbf{f}(\mathbf{p}^0) = \mathbf{0}$, we obtain upon equating the $\mathscr{O}(1)$ terms that

$$\mathbf{J}\mathbf{p}^1 = \mathbf{p}_t^0 - M\mathbf{p}^0. \tag{23}$$

By Assumption 3.2, we have the existence of a unique (up to scalar multiple) ϕ such that $\mathbf{J}\phi = \mathbf{0}$. Since the eigenvalues of $\mathbf{J}$ and $\mathbf{J}^T$ are identical, $\lambda = 0$ is also an eigenvalue of $\mathbf{J}^T$ of multiplicity one. This guarantees the existence of a unique (up to scalar multiple) ψ such that $\psi^T\mathbf{J} = \mathbf{0}^T$. In fact, we readily identify that $\psi = (1, \ldots, 1)^T$, as a result of the fact that (2) holds. From the Fredholm alternative, a solution to (23) exists if and only if $\psi^T(\mathbf{p}_t^0 - M\mathbf{p}^0) = 0$. This solvability condition yields

$$\psi^T\mathbf{p}_t^0 = \psi^T M\mathbf{p}^0, \tag{24a}$$

which is a scalar nonlinear PDE for $\alpha(x,t)$. This PDE (24a) for $\alpha(x,t)$ is called the QSS PDE, and the boundary conditions for α can be readily obtained from a conservation condition (see the examples in Sects. 4.1, 4.2, 4.3 below). In terms of $\alpha(x,t)$, the leading-order asymptotics

$$\mathbf{p} \sim \mathbf{p}^0(\alpha(x,t)) + \mathscr{O}(\varepsilon), \tag{24b}$$

then provides an approximate solution to the full system (15) when $t = \mathscr{O}(1)$ and away from any boundary layers near the endpoints $x = 0, 1$. The system (24b) is supplemented by appropriate boundary conditions (BCs). For the three-component molecular motors systems of Sect. 4, we present appropriate BCs below and carry out a boundary layer analysis in "Appendix D".

We remark that for the case where $\mathbf{f}$ is linear, as studied in Newby and Bressloff (2010b) and Dauvergne and Edelstein-Keshet (2015), the $\mathscr{O}(\varepsilon)$ term in (24b) can be calculated explicitly. However, in our extension of the theory to allow for a nonlinear $\mathbf{f}$, it is in general analytically intractable to calculate this correction term.

4 Examples of the QSS Theory

We now apply our QSS reduction method to the molecular motor models that were described in Sect. 2.

4.1 QSS Reduction: Kinesin Model

As shown in "Appendix B.3", the kinesin model (3) of Sect. 2.1 can be scaled to a system of the form (15) where

$$\mathbf{p} = \begin{pmatrix} p^{\mathrm{R}} \\ p^{\mathrm{L}} \\ p^{\mathrm{U}} \end{pmatrix}, \qquad \mathbf{f}(\mathbf{p}) = \begin{pmatrix} k_{\mathrm{a}} P(x) g(p^{\mathrm{U}}) - p^{\mathrm{R}} \\ k_{\mathrm{a}}(1 - P(x)) g(p^{\mathrm{U}}) - p^{\mathrm{L}} \\ -k_{\mathrm{a}} g(p^{\mathrm{U}}) + p^{\mathrm{R}} + p^{\mathrm{L}} \end{pmatrix},$$
$$\mathbf{M} = \begin{pmatrix} -\frac{\partial}{\partial x} & 0 & 0 \\ 0 & \frac{\partial}{\partial x} & 0 \\ 0 & 0 & D\frac{\partial^2}{\partial x^2} \end{pmatrix}, \tag{25}$$

where D and ε are defined in (82), while k_{a} is defined in (78) if g is linear and in (82) if g is either a Hill or Michaelis–Menton nonlinearity. The parameter k_{a} involves the ratio $k_{\mathrm{b}}/k_{\mathrm{u}}$. For the case of unbiased MT distribution ($P = 0.5$) and linear binding function g, we have, simply, $k_{\mathrm{a}} = k_{\mathrm{b}}/k_{\mathrm{u}}$, which represents the ratio of time spent in the unbound (diffusive) state to the time spent in the bound state (directed motor motion on MTs). As shown in (82), if g is nonlinear, then that ratio gets modified by the saturation factor, favouring the unbound residence time due to a limited number of binding sites.

Following the method described in Sect. 3, we first find the quasi-steady-state $\mathbf{p}^0(\alpha)$ from the condition that $\mathbf{f} = \mathbf{0}$. We set $f_1 = f_2 = 0$ in (25) to get

$$p^{\mathrm{R}} = P(x) k_{\mathrm{a}} g(p^{\mathrm{U}}), \qquad p^{\mathrm{L}} = (1 - P(x))\, k_{\mathrm{a}} g(p^{\mathrm{U}}), \tag{26}$$

which are two nonlinear equations in three unknowns. It is convenient to parameterize the free variable by a scalar, and we set $p^{\mathrm{U}} = \alpha$. This gives the quasi-steady-state solution branch as

$$\mathbf{p}^0(\alpha) = \begin{pmatrix} P(x) k_{\mathrm{a}} g(\alpha) \\ (1 - P(x)) k_{\mathrm{a}} g(\alpha) \\ \alpha \end{pmatrix}, \tag{27}$$

where the parameter $\alpha = \alpha(x, t)$ is the unknown cytosolic motor density. A simple calculation of the Jacobian $\mathbf{J}$ in Definition 3.1 shows that $\mathbf{J}$ has the eigenvalues

$$\lambda = 0, \qquad \lambda = -1, \qquad \lambda = -1 - k_{\mathrm{a}} g'(\alpha). \tag{28}$$

Therefore, a sufficient condition for $\mathbf{p}^0$ to be a slow manifold in the sense of Definition 3.1 is that g is a monotonically increasing function. This makes sense and implies that the rate of motors binding to MT increases with the cytosolic motor concentration: the more motors are in the cytosol, the more binding can take place (increasing, possibly up to some saturation level).

To derive the QSS PDE for $\alpha(x,t)$, we use the solvability condition (24), which yields that

$$(1,1,1)\frac{\partial}{\partial t}\begin{pmatrix} P(x)k_{\mathrm{a}}g(\alpha) \\ (1-P(x))k_{\mathrm{a}}g(\alpha) \\ \alpha \end{pmatrix} = (1,1,1)\mathbf{M}\begin{pmatrix} P(x)k_{\mathrm{a}}g(\alpha) \\ (1-P(x))k_{\mathrm{a}}g(\alpha) \\ \alpha \end{pmatrix}.$$

By using (25) for the matrix differential operator $\mathbf{M}$, this expression reduces to

$$\frac{\partial}{\partial t}\left(k_{\mathrm{a}}g(\alpha)+\alpha\right) = -\frac{\partial}{\partial x}\left(P(x)k_{\mathrm{a}}g(\alpha)\right) + \frac{\partial}{\partial x}\left((1-P(x))k_{\mathrm{a}}g(\alpha)\right) + D\frac{\partial^2\alpha}{\partial x^2},$$

which yields the QSS PDE

$$\frac{\partial}{\partial t}\left(k_{\mathrm{a}}g(\alpha)+\alpha\right) = \frac{\partial}{\partial x}\left(D\frac{\partial\alpha}{\partial x} - (2P(x)-1)k_{\mathrm{a}}g(\alpha)\right). \tag{29}$$

As shown in (108) of "Appendix D", to determine the boundary conditions for (29), we need only substitute (21) into the original boundary conditions (5) and retain terms up to $\mathscr{O}(\varepsilon)$. This leads to

$$\left(D\frac{\partial\alpha}{\partial x} - (2P(x)-1)k_{\mathrm{a}}g(\alpha)\right)\Big|_{x=0,1} = 0, \tag{30}$$

which we identify as zero-flux boundary conditions for the QSS PDE (29). Moreover, by integrating the PDE (29) across the domain, and using the boundary conditions, we identify the QSS PDE as a conservation law for the total density of kinesin motors:

$$\frac{\partial}{\partial t}\int_0^1 y(x,t)\,\mathrm{d}x = \frac{\partial}{\partial t}\int_0^1 \left(k_{\mathrm{a}}g(\alpha)+\alpha\right)\,\mathrm{d}x = 0, \tag{31}$$

where, with $\mathbf{e} \equiv (1,\ldots,1)^T$, we have defined

$$y(x,t) \equiv \mathbf{e}^T\mathbf{p}^0(\alpha(x,t)) = k_{\mathrm{a}}g(\alpha(x,t)) + \alpha(x,t), \tag{32}$$

as the total density of kinesin motor in any state at (x,t). Therefore, from (31), we have $\int_0^1 y(x,t)\,\mathrm{d}x = \int_0^1 y(x,0)\,\mathrm{d}x$.

The QSS PDE (29) describes the bulk behaviour of cytosolic motors, $p^{\mathrm{U}} = \alpha$, throughout the cell, but any from any boundary layers near the domain endpoints, when $\varepsilon \ll 1$. In terms of α, we can use (27) in (24b) to determine the behaviour of the densities of right- and left-moving kinesin motors in the bulk region away from any boundary layers near either $x = 0$ or $x = 1$. The boundary layer analysis, given in "Appendix D", and summarized in (113) for the kinesin model, shows that the right-moving and left-moving motors have a classic boundary layer

structure near $x = 0$ and $x = 1$, respectively, with a boundary layer width of $\mathscr{O}(\varepsilon)$.

In the case where $P(x) = P$ is constant, the QSS PDE (29) reduces to

$$\frac{\partial \alpha}{\partial t} = \mathscr{V}(\alpha)\frac{\partial \alpha}{\partial x} + \mathscr{D}(\alpha)\frac{\partial^2 \alpha}{\partial x^2}, \tag{33a}$$

where the effective velocity $\mathscr{V}(\alpha)$ and effective diffusion coefficients $\mathscr{D}(\alpha)$ are defined by

$$\mathscr{V}(\alpha) \equiv \frac{(1-2P)k_a g'(\alpha)}{k_a g'(\alpha)+1}, \qquad \text{and} \qquad \mathscr{D}(\alpha) \equiv \frac{D}{k_a g'(\alpha)+1}. \tag{33b}$$

If $P(x)$ is a smooth spatially varying function, then an additional nonlinear source term in α, proportional to $P'(x)$, would appear in (33a).

For a general $g(\alpha)$, we can use the QSS PDE (33) to make predictions regarding the bulk behaviour of the motors within the cell. The effective velocity and effective diffusion coefficients $\mathscr{V}(\alpha)$ and $\mathscr{D}(\alpha)$ are velocity and diffusion coefficients weighted by the fraction of time spent in directed (motor) and random (diffusive) motion, respectively. These effective velocity and diffusion coefficients depend on the model parameters as follows.

A bias in the MT polarity proportion, P, results in a corresponding bias in the effective velocity $V(\alpha)$, in such a way that $V(\alpha)$ is positive when $P > \frac{1}{2}$ and is negative when $P < \frac{1}{2}$. Although α represents the density of cytosolic motors, it influences the behaviour in the other states due to the assumption of rapid transitions between states. This bias agrees with the intuition that in areas where more MTs are biased to the right, more motors will be directed towards the right end of the cell. When the MT polarity is unbiased, i.e. $P = \frac{1}{2}$, then the QSS PDE (33) reduces, as expected, to a nonlinear diffusion equation with no advection.

In addition, when $g(\alpha)$ is monotone increasing, $V(\alpha)$ is a saturating function of k_a and $\mathscr{D}(\alpha)$ is a saturating function of $1/k_a$. Increasing k_b, which corresponds to increasing k_a, increases the effective velocity $\mathscr{V}(\alpha)$, while decreasing the effective diffusion coefficient $\mathscr{D}(\alpha)$. Similarly, increasing k_u, which decreases k_a, causes an increase in the effective diffusion, but decreases the effective velocity. In the molecular motor system when $k_b \gg k_u$, so that $k_a \gg 1$, we expect advective processes to dominate over diffusion as motors spend more time being transported on MTs than diffusing in the cytosol. Conversely, when $k_u \gg k_b$, so that $k_a \ll 1$, we expect diffusion to dominate over advective processes, as the motors spend less time walking on MTs than diffusing in the cytosol. The parameter dependence of $V(\alpha)$ and $\mathscr{D}(\alpha)$ on k_a in the QSS PDE (33) reflects this trade-off.

In the following subsections, we will explore how specific choices of the interaction function $g(\alpha)$ and the MT polarity $P(x)$ affect the QSS PDE, and further explore the parameter dependencies discussed briefly above.

4.1.1 Saturated Binding Model

We now study the kinesin model with a saturated binding rate, where we take

$$g(\alpha) \equiv \frac{\alpha}{1 + c\alpha}. \tag{34}$$

This choice models the basic Michaelis–Menten biochemical kinetics with $1/c$ representing the motor density at which the binding rate is 1/2 of its maximal magnitude. This choice of g represents the idea that binding sites on MTs are limited. As cytosolic motor density α increases, those MT sites become saturated so that $g \to 1$. When $c = 0$, the binding rate is linear and the model reduces to that studied in Dauvergne and Edelstein-Keshet (2015).

From (27), the quasi-steady-state $\mathbf{p}^0(\alpha)$ for this saturated binding kinesin model with constant polarity P is

$$\mathbf{p}^0(\alpha) = \begin{pmatrix} P\frac{k_a\alpha}{(1+c\alpha)} \\ (1-P)\frac{k_a\alpha}{(1+c\alpha)} \\ \alpha \end{pmatrix}. \tag{35}$$

Since $g(\alpha)$ is monotone increasing, the condition in Definition 3.1 holds, and $\mathbf{p}^0(\alpha)$ is a slow manifold. Therefore, from (29), the QSS PDE for $\alpha(x,t)$ reduces to

$$\frac{\partial}{\partial t}\left(\frac{k_a\alpha}{(1+c\alpha)} + \alpha\right) = \frac{\partial}{\partial x}\left(D\frac{\partial \alpha}{\partial x} - (2P-1)\frac{k_a\alpha}{(1+c\alpha)}\right). \tag{36}$$

Using (30), and as shown in (108) of "Appendix D", this QSS PDE inherits its zero-flux boundary conditions from the full system as

$$D\frac{\partial \alpha}{\partial x} - (2P-1)\frac{k_a\alpha}{(1+c\alpha)} = 0, \qquad \text{at} \quad x = 0, 1. \tag{37}$$

We compare the QSS approximation with numerical approximations of the full kinesin model (15) with (25) and (34). For a correct comparison, the initial condition $\alpha(x,0) = \alpha_0$ needs to be chosen such that the total density y is the same for the full system and the QSS PDE. Conservation of mass with the initial condition $p^{\mathrm{R}} = 0$, $p^{\mathrm{L}} = 0$ and $p^{\mathrm{U}} = 1$ at $t = 0$ for the full system implies that

$$\int_0^1 \left(p^{\mathrm{R}}(x,t) + p^{\mathrm{L}}(x,t) + p^{\mathrm{U}}(x,t)\right) \mathrm{d}x = 1, \tag{38}$$

for all t. Recall that the QSS PDE is a conservation law for

$$y(x,t) = \mathbf{e}^T\mathbf{p}^0(\alpha(x,t)) = k_a g(\alpha) + \alpha, \tag{39}$$

which is the total density of kinesin in the cell. Therefore, one correct initial condition is to choose α_0 to be the unique root of

$$y(x,0) = k_a g(\alpha_0) + \alpha_0 = 1. \tag{40}$$

The steady-state solution $\alpha(x)$ of the QSS PDE (36) is the solution to the non-local problem

$$\frac{\partial \alpha}{\partial x} = \frac{k_a}{D}(2P-1)g(\alpha), \qquad \int_0^1 (k_a g(\alpha) + \alpha)\, \mathrm{d}x = 1, \tag{41}$$

where $g(\alpha)$ is defined in (34). There are a few special cases for which explicit solutions to (41) can be found. In particular, when $P = 0.5$, so that $\alpha = \alpha_c$, where α_c is a constant, we readily obtain from (41) that

$$\begin{aligned} \alpha_c &= \frac{1}{k_a+1}, \quad (c=0)\,; \\ \alpha_c &= \frac{1}{2c}\left(c - (k_a+1) + \sqrt{(c-(k_a+1))^2 + 4c}\right), \quad (c>0). \end{aligned} \tag{42}$$

For the linear binding case, where $k_a = k_b/k_u$, we observe that the expression for α_c is

$$\alpha_c = \frac{\frac{1}{k_b}}{\frac{1}{k_u} + \frac{1}{k_b}},$$

which represents the fraction of time spent in the unbound state (k_b gives the rate at which a freely diffusing motor binds to MTs, so $\frac{1}{k_b}$ gives the mean residence time in the unbound state). In addition, for linear binding where $c = 0$ so that $g(\alpha) = \alpha$, then $\alpha(x) = \alpha_c e^{\beta x}$ where $\beta \equiv (2P-1)k_a/D$. By substituting this form into the non-local condition of (41), we readily calculate α_c to obtain for linear binding that

$$\alpha(x) = \alpha_c e^{\beta x}, \qquad \text{where} \qquad \alpha_c = \frac{\beta}{k_a+1}\frac{1}{e^{\beta}-1}, \qquad \beta = \frac{(2P-1)k_a}{D}. \tag{43}$$

When the MT polarity $P \neq 0.5$ is also constant across the cell, this case reduces to simple exponential distributions of all kinesin states; that distribution is biased towards the left ($P < 0.5$) or towards the right ($P > 0.5$), as previously described in Dauvergne and Edelstein-Keshet (2015). However, in general, the solution to the non-local problem (41) must be obtained numerically. As shown in "Appendix C", by recasting this non-local problem into an initial value problem, its solution can be computed using a simple numerical shooting procedure.

In Fig. 3a–d we plot numerical approximations of the steady-state solution to the full transport model (dashed) and the QSS PDE (solid) for both linear binding ($c = 0$) and saturated nonlinear binding ($c = 1$), for two constant values of the MT polarity. For $P = 0.5$, and for $c = 0$ and $c = 1$, the advection term in (33) vanishes, leaving a purely

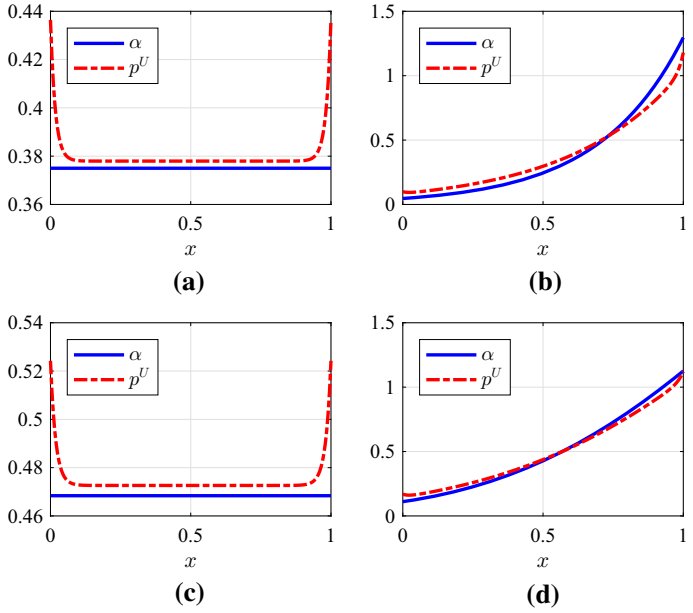

Fig. 3 Effect of nonlinear binding and microtubule polarity. A comparison for $P = 0.5$ (unbiased MT polarity, *left panels*) and for $P = 0.6$ (MT biased to the right, *right panels*) of the steady-state cytosolic density $p^{\mathrm{U}}(x)$ (*dashed curves*) of the full model (15), (25), and (34), with the steady-state $\alpha(x)$ (*solid curves*) from the QSS PDE (36). **a**, **b** Linear binding ($c = 0$) [results in agreement with Dauvergne and Edelstein-Keshet (2015)]. **c**, **d** Saturated nonlinear binding with $c = 1$. The parameters are $k_{\mathrm{a}} = 5/3$, $\varepsilon = 0.02$, and $D = 0.1$. The total mass was initially fixed at $\int_0^1 y(x,t)\,\mathrm{d}x = 1$ and is preserved in time. Notice the different *vertical scales* between **a** and **c**. The QSS approximation describes the bulk behaviour of the system well, but does not capture the boundary behaviour

diffusive motion. For $P = 0.6$, the MT polarity is biased to the right. Consequently, the distributions of bound and cytosolic motors are also biased towards the right end of the cell at $x = 1$. From Figure 3c, d we observe that the saturated binding term with $c = 1$ slows the rate at which kinesin leaves the cytosolic compartment, causing more kinesin to be sequestered in the middle of the cell. We further observe that the QSS approximation is not valid in thin boundary layers near the two edges of the cell. These boundary layers result from the reduction of the full three-equation model with four boundary conditions, to a single PDE with two boundary conditions. The results from the boundary layer analysis given in (113) of "Appendix D" show that the unbound kinesin motor density p^{U} near the two boundaries differs from its outer approximation $p^{\mathrm{U}} \sim \alpha$ by an error $\mathcal{O}(\varepsilon/D)$.

In Fig. 4, we compare the steady-state solution to the QSS approximation in the linear binding ($c = 0$) and saturated binding case ($c = 1$), for the parameter range where $k_{\mathrm{a}} < 1$ (a) and $k_{\mathrm{a}} > 1$ (b) with $P = 0.6$. In general, saturated binding results in a shallower gradient of cytosolic motors across the cell. This result agrees with the intuition that saturated binding restricts the rate of binding for large motor density. This consequently restricts the total number of motors walking to the right end of the

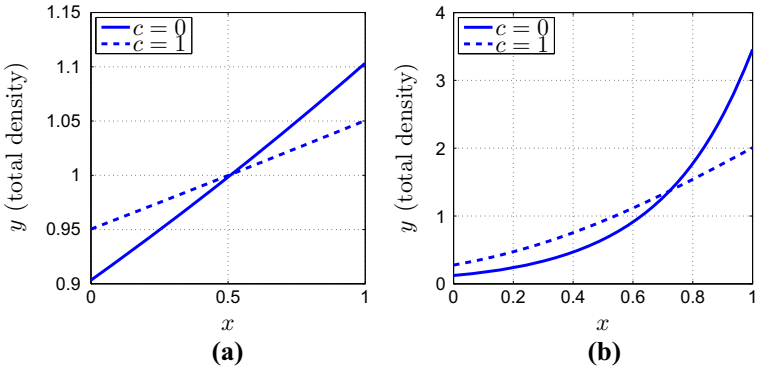

Fig. 4 Effect of the relative magnitudes of binding and unbinding rates $k_\mathrm{b}, k_\mathrm{u}$. Steady-state solutions $y(x) = \mathbf{e}^T \mathbf{p}^0(\alpha(x))$, obtained from the steady-state $\alpha(x)$ of the QSS PDE (36) with linear binding ($c = 0$, *solid*) and saturated binding ($c = 1$, *dashed*) when $k_\mathrm{a} < 1$ (**a**) and $k_\mathrm{a} > 1$ (**b**). The other parameters are $P = 0.6$, and $D = 0.1$, and the total mass was $\int_0^1 y(x)\,\mathrm{d}x = 1$. In general, saturated binding results in a shallower gradient of motors across the cell. The steady-state behaviour illustrates the effects of k_b and k_u. For example, for large k_u (relative to k_b) as in **a** where $k_\mathrm{a} = 0.1$, the effective velocity, $V(\alpha)$, is much smaller than the effective diffusion coefficient, $\mathscr{D}(\alpha)$. This leads to a comparatively more uniform density of motors than in **b**, where k_b is larger than k_u, and the advection term dominates

cell ($P = 0.6$), and in turn, saturated binding restricts the total number of motors that accumulate at the cell end.

4.1.2 Saturated Binding with a Spatially Variable MT Polarity

Next, we consider a spatially varying MT polarity throughout the cell, $P = P(x)$, and derive a QSS approximation for the corresponding system of transport equations for the case of saturated binding. In this case, the quasi-steady-state $\mathbf{p}^0(\alpha)$ is

$$\mathbf{p}^0(\alpha) = \begin{pmatrix} P(x)k_\mathrm{a}g(\alpha) \\ (1-P(x))k_\mathrm{a}g(\alpha) \\ \alpha \end{pmatrix}, \qquad g(\alpha) = \frac{\alpha}{1+c\alpha}. \tag{44}$$

The QSS PDE, from (29), is

$$\frac{\partial}{\partial t}\left(\frac{k_\mathrm{a}\alpha}{(1+c\alpha)} + \alpha\right) = \frac{\partial}{\partial x}\left(D\frac{\partial \alpha}{\partial x} - (2P(x)-1)\frac{k_\mathrm{a}\alpha}{(1+c\alpha)}\right). \tag{45}$$

We observe that the sign of the advection term depends only on the sign of $(2P(x)-1)$. If $P(x) < 0.5$, then advection is to the left, while if $P(x) > 0.5$, then advection is to the right. Biologically, if the MT polarity changes across the cell, we expect the bulk molecular motor behaviour to change correspondingly. If $P(x) > 0.5$ on some subinterval, we interpret the MT bias to be to the right. This leads to a collection of motors walking to the right in this subinterval. Moreover, if $P(x) < 0.5$ on some subinterval, then the bulk movement of motors in this subinterval is to the left.

To explore the effect of non-constant $P(x)$ on the QSS PDE (45) we consider two hypothetical MT polarity functions. Our first choice is

$$P(x) = \frac{1}{2}\left[1 - \tanh\left(x - \frac{1}{2}\right)\right], \tag{46}$$

for which $P(0) \approx 1$, $P(1) \approx 0$, $P(\frac{1}{2}) = \frac{1}{2}$, and $P'(x) = -\frac{1}{2}\,\mathrm{sech}^2(x - \frac{1}{2})$. For $x \in [0, \frac{1}{2})$, we have $P(x) > \frac{1}{2}$, which indicates that the MT polarity is biased to the right in the left part of the cell. Similarly, for $x \in (\frac{1}{2}, 1]$, we have $P(x) < \frac{1}{2}$, which indicates that the MT polarity is biased to the left in the right part of the cell. As a result of this MT polarity bias, the effective velocity coefficient in the QSS PDE changes signs at $x = \frac{1}{2}$. We expect kinesin to walk towards the centre of the cell and become "trapped" there. In Fig. 5a, we observe an aggregation of kinesin motors in the centre of the cell at steady-state as predicted by the QSS PDE for both linear ($c = 0$) and saturated binding ($c = 1$). The steady-state problem is solved numerically by the shooting method outlined in "Appendix C".

Following Dauvergne and Edelstein-Keshet (2015) and Gou et al. (2014), where molecular motor movement in the hyphae of the fungus *Ustilago maydis* was studied, our second choice is to consider a MT polarity bias near $x = 0$ and $x = 1$ that is polarized towards these cell ends, while the MTs near the cell centre point to the right and to the left with (roughly) equal probability. As a model of such a polarity we take

$$P(x) = \frac{1}{2}\left(1 + \tanh\left[2\left(x - \frac{1}{2}\right)\right]\right). \tag{47}$$

From the numerical computations of the steady-state of the QSS PDE, as shown in Fig. 5b, we observe that with such a $P(x)$ most of the kinesin motors are pushed towards the boundaries of the cell for both linear ($c = 0$) and saturated binding ($c = 1$). This results from the highly left-biased region at the left end of the cell and the highly right-biased region at the right end of the cell. Moreover, saturated binding sequesters more kinesin in the cytosolic compartment in the middle of the cell with a nonzero density persisting throughout the cell at steady-state.

4.1.3 Hill Function Binding

Next, we consider a general Hill function for the binding rate, $g(\alpha)$, given by

$$g(\alpha) = \frac{\alpha^n}{K^n + \alpha^n}, \tag{48}$$

where $n \geq 1$ and $K > 0$. Hill functions with $n \geq 2$ are typically used to model positive feedback or cooperative binding in biological systems. In this case, we can think of kinesin motors binding cooperatively to the MTs in such a way that for low densities of motors the binding rate is slow, at intermediate densities ($\alpha \approx K$) binding is rapid, while for high densities of motors the binding rate saturates to some maximal level.

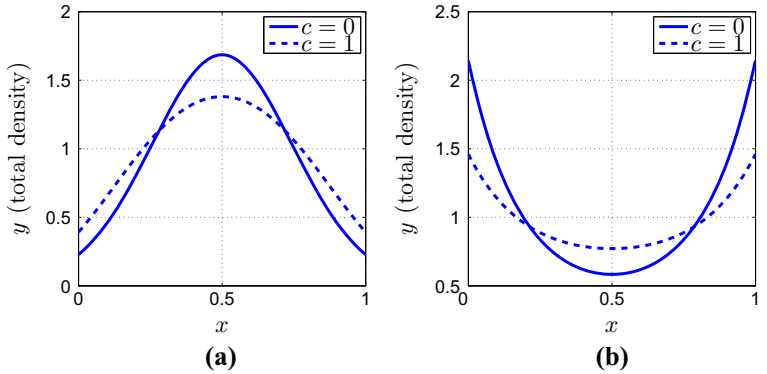

Fig. 5 Effects of two spatially dependent MT bias functions, $P(x)$. Steady-states $y(x) = \mathbf{e}^T \mathbf{p}^0(\alpha(x))$, obtained from the steady-state $\alpha(x)$ of the QSS PDE (45) with spatially varying MT polarity where **a** MTs "point towards" the cell centre (described by $P(x)$ in (46)) and **b** "point towards" the cell ends ($P(x)$ as given in (47)). In both panels we show linear ($c = 0$, *solid*) and saturated binding ($c = 1$, *dashed*). In **a** we observe an accumulation of kinesin at the centre of the cell, whereas in **b** the accumulation is at the cell ends. Saturated binding sequesters more kinesin motors in the cytosolic compartment, which results in the shallower, diffusion-dominated, motor distributions in the case $c = 1$ in both **a** and **b**. Other parameters are $k_a = 5/3$, and $D = 0.1$. The total mass was fixed at $\int_0^1 y(x)\,\mathrm{d}x = 1$. **a** $P(x) = \frac{1}{2}\left(1 - \tanh\left(x - \frac{1}{2}\right)\right)$, **b** $P(x) = \frac{1}{2}\left(1 + \tanh\left(x - \frac{1}{2}\right)\right)$

The parameter K describes the value of α at which $g(\alpha)$ reaches half of its maximum value, while the parameter n describes the "sharpness" of the switch.

With this choice (48) of monotonically increasing $g(\alpha)$, the quasi-steady-state slow manifold is given in terms of $g(\alpha)$ by (44). In addition, the QSS PDE is given by (29) with boundary conditions (30). We now numerically examine the role of the Hill parameters n and K and discuss the effects that these parameters have on the bulk behaviour of kinesin within the cell.

In Fig. 6, we show numerical approximations to the steady-state solution of the QSS PDE for different values of n and K when P is fixed at $P = 0.6$. In particular, in Fig. 6a, steady-state solutions are shown for a fixed $K = 1$ and for increasing n. Since at motor density $\alpha = K$ the binding rate is half-maximal, we note that $g(\alpha) < \frac{1}{2}$ for $\alpha < K$. This implies that the advection term, $k_a(2P-1)g(\alpha)$, remains relatively small for $\alpha < K$. This makes sense, since motors hardly bind to MT at that low density. As K decreases from panel (a)–(c) in Fig. 6, the switch to rapid binding is made possible wherever α exceeds K. For $\alpha > K$, the advection term is near maximal, and we consequently observe an aggregation of kinesin motor at the right end of the cell. Hence, decreasing K from the value 1 shifts the system from slow advection to fast advection, as seen by a comparison of the bulk distribution of motors across the cell in panels (a)–(c). The parameter n controls the "sharpness" of the transition zone near $\alpha \approx K$ in the Hill function. As n increases, the approximation $g(\alpha) \approx 0$ for $\alpha < K$ and $g(\alpha) \approx 1$ for $\alpha > K$ improves. In Fig. 6b we set $K = 0.5$. As n increases, the switch from slow advection to fast advection becomes shaper. Hence, for large n, in regions where the cytosolic motor density α is larger than K, advection dominates over diffusion. Increasing n results in a sharper distribution of motors across the cell in the steady-state solution.

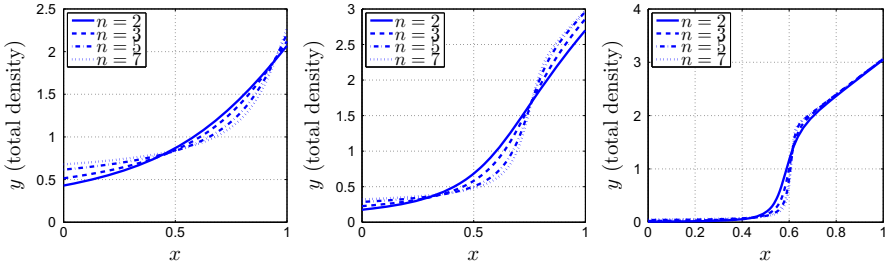

Fig. 6 Effect of the Hill function parameters K and n. Steady-states $y(x) = \mathbf{e}^T \mathbf{p}^0(\alpha(x))$, obtained from the steady-state $\alpha(x)$ of the QSS PDE (45) with a Hill function binding rate (48) for $P = 0.6$. The parameter K represents the density of motors p^{U} that leads to $g(p^{\mathrm{U}}) = 1/2$, whereas the Hill coefficient n governs the "sharpness" of the Hill function. Other parameters are $k_{\mathrm{a}} = 5/3$ and $D = 0.1$. The total mass was fixed at $\int_0^1 y(x)\,\mathrm{d}x = 1$. **a** $K = 1$, **b** $K = 0.5$ and **c** $K = 0.1$

4.2 QSS Reduction: Kinesin–Dynein Model

As shown in "Appendix B.4", the kinesin–dynein model (8) of Sect. 2.2 can be scaled to a system of the form (15), where we identify

$$\mathbf{p} = \begin{pmatrix} p^{\mathrm{R}} \\ p^{\mathrm{L}} \\ p^{\mathrm{U}} \end{pmatrix}, \qquad \mathbf{f}(\mathbf{p}) = \begin{pmatrix} k_{\mathrm{a}} Q p^{\mathrm{U}} - p^{\mathrm{R}} - k p^{\mathrm{R}} p^{\mathrm{L}} \\ k_{\mathrm{a}}(1-Q) p^{\mathrm{U}} - p^{\mathrm{L}} + k p^{\mathrm{R}} p^{\mathrm{L}} \\ p^{\mathrm{R}} + p^{\mathrm{L}} - k_{\mathrm{a}} p^{\mathrm{U}} \end{pmatrix},$$
$$\mathbf{M} = \begin{pmatrix} -\frac{\partial}{\partial x} & 0 & 0 \\ 0 & v\frac{\partial}{\partial x} & 0 \\ 0 & 0 & D\frac{\partial^2}{\partial x^2} \end{pmatrix}. \tag{49}$$

Here the positive dimensionless parameters v, k_{a}, k, and D are defined in terms of the original parameters of (8) by

$$v \equiv \frac{v_{\mathrm{l}}}{v_{\mathrm{r}}}, \qquad D \equiv \frac{D_0}{v_{\mathrm{r}} L_0}, \qquad \varepsilon \equiv \frac{v_{\mathrm{r}}}{k_{\mathrm{u}} L_0}, \qquad k_{\mathrm{a}} \equiv \frac{k_{\mathrm{b}}}{k_{\mathrm{u}}}, \qquad k \equiv \frac{k_{\mathrm{c}}\rho}{k_{\mathrm{u}}} = \frac{(k_{\mathrm{rl}} - k_{\mathrm{lr}})\rho}{k_{\mathrm{u}}}. \tag{50}$$

Without loss of generality, we assume that $k_{\mathrm{rl}} > k_{\mathrm{lr}}$, so that $k > 0$, since the cell ends are interchangeable. It is convenient to parameterize the quasi-steady solution in terms of $p^{\mathrm{L}} = \alpha$. In "Appendix B.4", we readily determine that there is a unique quasi-steady-state solution satisfying $\mathbf{f} = \mathbf{0}$ given by

$$\mathbf{p}^0(\alpha) = \begin{pmatrix} p^{\mathrm{R}} \\ p^{\mathrm{L}} \\ p^{\mathrm{U}} \end{pmatrix} = \begin{pmatrix} \frac{Q\alpha}{k\alpha + 1 - Q} \\ \alpha \\ \frac{1}{k_{\mathrm{a}}}\left(\alpha + \frac{Q\alpha}{k\alpha + 1 - Q}\right) \end{pmatrix}. \tag{51}$$

To determine whether this quasi-steady-state solution is a slow manifold in the sense of Definition 3.1 we must calculate the eigenvalues λ of the Jacobian of $\mathbf{f}$ at

$\mathbf{p} = \mathbf{p}^0$. From a straightforward calculation we obtain that $\lambda = 0$ and that the other two eigenvalues $\lambda_\pm$ satisfy the quadratic equation

$$\lambda^2 - \sigma_1\lambda + \sigma_2 = 0\,; \qquad \sigma_1 \equiv -2 - k_a + k\left(p^R - p^L\right),$$
$$\sigma_2 \equiv 1 + k_a + k(1+k_a)(p^L - p^R). \tag{52}$$

By using (51) for p^L and p^R, we determine σ_1 and σ_2 explicitly as

$$\sigma_1 = -2 - k_a - k\alpha H(Q), \quad \sigma_2 = 1 + k_a + k\alpha(1+k_a)H(Q);$$
$$\text{where} \quad H(Q) \equiv 1 - \frac{Q}{1+k\alpha-Q}. \tag{53}$$

A necessary and sufficient condition for $\mathrm{Re}(\lambda_\pm) < 0$ is that $\sigma_1 < 0$ and $\sigma_2 > 0$ in (53). In "Appendix B.4" we show that these inequalities hold for any Q on $0 \le Q \le 1$. Therefore, $\mathbf{p}^0$ is a slow manifold in the sense of Definition 3.1.

Next, to determine the QSS PDE for $\alpha(x,t)$ governing the dynamics on the slow manifold we simply calculate the terms in the solvability condition (24a). This leads to the QSS PDE for $\alpha(x,t)$, given by

$$\frac{\partial}{\partial t}\left(\left(1+\frac{1}{k_a}\right)\left(\frac{k\alpha+1}{k\alpha+1-Q}\right)\alpha\right) = \frac{\partial}{\partial x}\left(\mathscr{V}(\alpha)\alpha + \mathscr{D}(\alpha)\frac{\partial\alpha}{\partial x}\right), \tag{54a}$$

where the "effective transport rate" and the "effective rate of diffusion" are given by

$$\mathscr{V}(\alpha) = \left(v - \frac{Q}{k\alpha+1-Q}\right), \qquad \mathscr{D}(\alpha) = \frac{D}{k_a}\left(1 + \frac{(1-Q)Q}{(k\alpha+1-Q)^2}\right), \tag{54b}$$

together with the zero-flux boundary conditions [see (108) of "Appendix D"]

$$\mathscr{V}\alpha + \mathscr{D}\frac{\partial\alpha}{\partial x} = 0, \qquad \text{at} \quad x = 0, 1. \tag{54c}$$

In Fig. 7 we compare numerical results for the motor densities p^R, p^L, and the total density y, in the steady-state solution of the full transport model [(15) and (49) with $\varepsilon = 0.02$] and in the corresponding steady-state of the QSS PDE (54). As shown, the full solution and the QSS solution agree well in the middle of the cell, but, as before, the QSS does not capture the boundary layer behaviour near the cell ends. "Appendix D.2" provides a qualitative phase-plane analysis of the boundary layer solutions and, in particular, predicts that $p^R \approx 0.82$ at $x = 1$, which agrees well with the result in Fig. 7a.

We now examine the behaviour of solutions to the QSS PDE (54) and the role of the parameters in the original model. We first observe from (51) that the density of freely diffusing motors is a weighted average of the left-moving and right-moving motors with weight $1/k_a$ (ratio of mean time spent bound to mean time spent freely diffusing). The density of right-moving motors at QSS, given by $\frac{Q\alpha}{k\alpha+1-Q}$, saturates

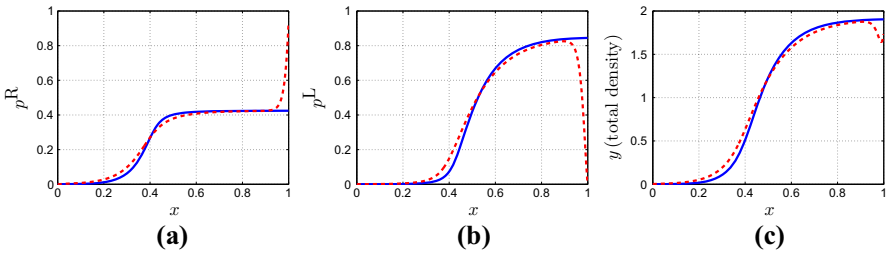

Fig. 7 Comparison of the full solution with the QSS solution. Shown are the steady-state of the full model (15) and (49) (*dashed curve*) for $\varepsilon = 0.02$ and the solution of the QSS PDE (54) (*solid curve*) for p^R (**a**), p^L (**b**), and the total density y at position x. The parameters are $D = 0.1$, $k_a = 2$, $k = 2$, $Q = 0.9$, and $v = 0.5$. The total mass in the cell was fixed at $\int_0^1 y(x)\,dx = 1$. The QSS approximation agrees well with the full solution except near the boundary layers at the ends of the cell. **a** p^R versus x. **b** p^L versus x. **c** y versus x

up to Q/k, as the density of left-moving motors, α, increases. From (54a) the sign of the effective transport velocity $\mathscr{V}$ in (54b) determines the direction of motion, with the motion being to the left if this quantity is positive. We readily calculate that the net movement is to the left when the density of left-moving motors, α, exceeds a threshold, i.e. when $\alpha > \frac{v(Q-1)+Q}{vk}$. For example, with fixed v and k, changing Q (which is the probability that a freely diffusing motor complex binds into the right-moving state) will change this condition. Lowering Q increases the probability that a freely diffusing motor binds into the left-moving state, which should bias the net advection to the left. The "effective diffusivity" $\mathscr{D}$ of the system in (54b) is influenced by the parameters D, k_a, k, and Q. Increasing k_a decreases the effective diffusion coefficient in (54a), which should lead to steeper solution profiles across the cell (as usual, increasing D has the opposite effect). Increasing the turning parameter k also decreases the diffusivity of the motors. The binding bias parameter Q appears in the diffusion coefficient in two ways. First, as $Q \to 0$ or $Q \to 1$, the diffusion coefficient approaches the limiting value D/k_a. Second, there exists a critical Q value that maximizes the effective rate of diffusion, given a fixed motor density α and fixed k (this critical Q value is $\frac{k\alpha+1}{2\alpha k+1}$).

In Fig. 8, we plot steady-state solutions to the QSS PDE (54) for a range of values of several parameters. These steady-states are readily calculated numerically by using a numerical shooting method (see "Appendix C"). The top labelled curve in panel (a) is produced with a baseline parameter set ($k = 2$, $k_a = 2$, $D = 0.1$, $v = 0.5$, $Q = 0.9$) to which parameter variations can be compared. The total mass of kinesin–dynein complex is fixed as $\int_0^1 y(x)\,dx = 1$, where $y(x) = \mathbf{e}^T\mathbf{p}^0(\alpha(x))$ and $\mathbf{p}^0$ is defined in (51). Decreasing the probability, Q, of binding to the right-moving state (panel (a)) allows for more freely diffusing motors to bind to the left-moving state, and a shift in right-biased movement to left-biased movement. Increasing the velocity ratio of left-moving to right-moving motor complexes v (panel (b)) biases net movement towards the left end of the cell, as expected. In (c), an increase in k_a, which decreases the "effective diffusivity" $\mathscr{D}$, sharpens the interface between the regions of high density and low density of stalled motors. In (d), increasing the turning rate constant, k, also biases the net movement to the left end of the cell. Note that high values of k are required to shift the behaviour from right-biased to left-biased due to the high baseline Q value ($Q = 0.9$).

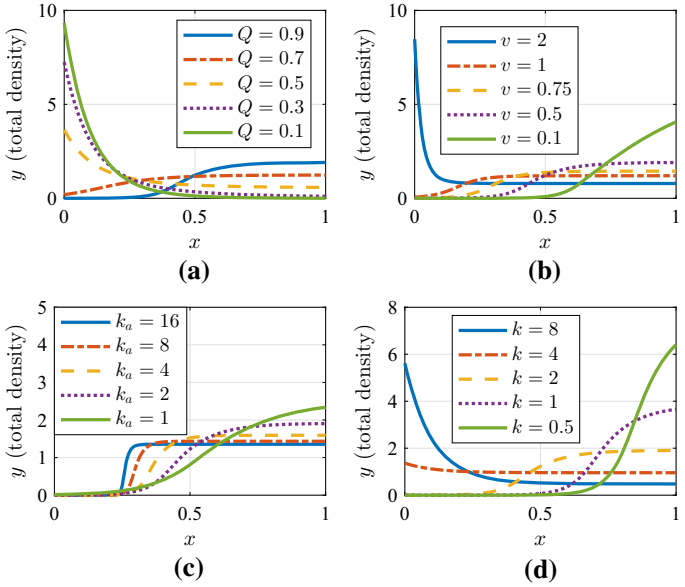

Fig. 8 The effect of parameters Q, v, k_a, k on the total density. The total density is $y(x) = \mathbf{e}^T \mathbf{p}^0(\alpha(x))$, obtained from the steady-state $\alpha(x)$ of the QSS PDE (54). Baseline parameters are $k = 2$, $k_a = 2$, $D = 0.1$, $v = 0.5$, $Q = 0.9$. This value of Q biases the bulk motor distribution to the right (top labelled curve in **a**). In **a**, decreasing the binding bias Q (probability of binding to the right) results in a shift in right-biased movement to left-biased movement. In **b**, an increase in v (the ratio of the velocities of left-moving to right-moving complexes) biases net movement towards the left. In **c**, an increase in k_a (which represents the ratio of binding to unbinding rates k_b/k_u) sharpens the interface between the regions of high density and low density of motors. In **d**, increasing the turning rate constant, k, also biases the net movement to the left end of the cell. The total mass was set to $\int_0^1 y(x)\,dx = 1$ (Color figure online)

4.3 QSS Reduction: Myosin Model

Next, we study the QSS reduction of the myosin model given in (90). The analysis of this model will differ from that of the previous two models in that there are two possible quasi-steady-state solutions. In addition, the boundary layer behaviour will play a non-trivial role in the dynamics.

As shown in "Appendix B.5", the myosin model (11) of Sect. 2.3 can be scaled to a system of the form (15) by

$$\mathbf{p} = \begin{pmatrix} p^{\mathrm{W}} \\ p^{\mathrm{B}} \\ p^{\mathrm{U}} \end{pmatrix}, \qquad \mathbf{f}(\mathbf{p}) = \begin{pmatrix} -k_{\mathrm{bw}} \left(p^{\mathrm{B}}\right)^2 p^{\mathrm{W}} + k_{\mathrm{b}} p^{\mathrm{U}} - p^{\mathrm{W}} \\ k_{\mathrm{bw}} \left(p^{\mathrm{B}}\right)^2 p^{\mathrm{W}} - p^{\mathrm{B}} \\ p^{\mathrm{B}} + p^{\mathrm{W}} - k_{\mathrm{b}} p^{\mathrm{U}} \end{pmatrix},$$

$$\mathbf{M} = \begin{pmatrix} -\frac{\partial}{\partial x} & 0 & 0 \\ 0 & v\frac{\partial}{\partial x} & 0 \\ 0 & 0 & D\frac{\partial^2}{\partial x^2} \end{pmatrix}, \tag{55}$$

where the dimensionless parameters v, D, ε, k_{bw}, and k_{b} are defined by

$$v \equiv \frac{v_{\mathrm{b}}}{v_{\mathrm{w}}}, \qquad D \equiv \frac{D_{\mathrm{f}}}{v_{\mathrm{w}} L_0}, \qquad \varepsilon \equiv \frac{v_{\mathrm{w}}}{k_{\mathrm{u}} L_0}, \qquad k_{\mathrm{bw}} \equiv \frac{\hat{k}_{\mathrm{bw}} \rho^2}{k_{\mathrm{u}}}, \qquad k_{\mathrm{b}} \equiv \frac{\hat{k}_{\mathrm{b}}}{k_{\mathrm{u}}}. \quad (56)$$

We set the nonlinear kinetics in the scaled myosin model (90a) and (90c) to zero to obtain the two equations

$$k_{\mathrm{bw}} \left(p^{\mathrm{B}}\right)^2 p^{\mathrm{W}} - p^{\mathrm{B}} = 0, \qquad -k_{\mathrm{b}} p^{\mathrm{U}} + p^{\mathrm{B}} + p^{\mathrm{W}} = 0. \quad (57)$$

The two possible solutions to the first equation in (57) are $p^{\mathrm{B}} = 1/\left[k_{\mathrm{bw}} p^{\mathrm{W}}\right]$ and $p^{\mathrm{B}} = 0$. In the latter case, the motors equilibrate between freely diffusing and walking on MT, with no motors in the bound, stalled state. In the former case, there is some proportion of motors that are stalled. We analyse each of these cases in turn.

4.3.1 Type I Quasi-Steady-States: $p^B \equiv 0$

We first consider $p^{\mathrm{B}} \equiv 0$. We let p^{U} be the free parameter and set $p^{\mathrm{U}} = \beta(x,t)$. This yields the quasi-steady-state

$$\mathbf{p}^0(\beta) = \begin{pmatrix} p^{\mathrm{W}} \\ p^{\mathrm{B}} \\ p^{\mathrm{U}} \end{pmatrix} = \begin{pmatrix} k_{\mathrm{b}}\beta \\ 0 \\ \beta \end{pmatrix}. \quad (58)$$

For $\mathbf{p}^0$, we readily calculate that the eigenvalues λ of the Jacobian of the kinetics $\mathbf{f}(\mathbf{p})$ at $\mathbf{p} = \mathbf{p}^0$ are $\lambda = 0$, $\lambda = -1$, and $\lambda = -1 - k_{\mathrm{b}}$. Therefore, (58) is a slow manifold in the sense of Definition 3.1. From the QSS reduction approach of Sect. 3, the QSS PDE for $\beta(x,t)$ is calculated by expanding the solvability condition (24a). This yields the linear PDE

$$(k_{\mathrm{b}}+1)\frac{\partial \beta}{\partial t} = \frac{\partial}{\partial x}\left[D\frac{\partial \beta}{\partial x} - k_{\mathrm{b}}\beta\right], \quad 0 < x < 1; \qquad D\frac{\partial B}{\partial x} = k_{\mathrm{b}}\beta, \quad \text{on} \quad x = 0, 1. \quad (59)$$

The steady-state solution $\beta_s(x)$ of (59) having a unit mass, so that $\int_0^1 (k_{\mathrm{b}}+1)\beta\, dx = 1$, is simply

$$\beta_s(x) = \left(\frac{k_{\mathrm{b}}}{(k_{\mathrm{b}}+1)D}\right)\frac{e^{k_{\mathrm{b}}(x-1)/D}}{1 - e^{-k_{\mathrm{b}}/D}}, \quad (60)$$

which determines the steady-state as $\mathbf{p}^0[\beta_s(x)]$ from (58).

Moreover, since the time-dependent QSS PDE (59) is linear, it is readily solved by separation of variables as

$$\beta(x,t) = \beta_s(x) + e^{k_b x/D} \sum_{n=1}^{\infty} c_n e^{-\lambda_n D t/(k_b+1)} \Phi_n(x), \tag{61}$$

where c_n for $n \geq 1$ are coefficients defined in terms of the initial data $\beta(x,0)$. Here $\lambda = \lambda_n > 0$ and $\Phi = \Phi_n(x)$ are the positive eigenvalues and eigenfunctions of the Sturm–Liouville problem

$$\begin{aligned} &\left(w(x)\Phi'\right)' + \lambda w(x)\Phi = 0, \quad 0 < x < 1\,; \\ &\Phi'(0) = \Phi'(1) = 0, \quad w(x) \equiv e^{k_b x/D}. \end{aligned} \tag{62}$$

Since the myosin model (90) is linear when $p^B \equiv 0$, the boundary layer analysis near $x = 0$ and $x = 1$ is routine for this quasi-steady-state. At steady-state, and with $p^B = 0$ in (90), we find from (110) that there is no boundary layer near $x = 1$. By solving the boundary layer equations (111) near $x = 1$, we readily obtain the leading-order uniform steady-state approximation

$$\begin{aligned} &p^W = k_b A \left(e^{k_b x/D} - e^{-x/\varepsilon}\right), \qquad p^U = A e^{k_b x/D}, \qquad \text{where} \\ &A \equiv \frac{k_b}{D(k_b+1)} \frac{e^{-k_b/D}}{1 - e^{-k_b/D}}. \end{aligned} \tag{63}$$

We see from (63) that p^U is an exponentially increasing function. By comparison, p^W has a rapidly decaying correction factor (since $1/\varepsilon$ is large in the second exponential), which produces a small "knee" in its graph, Fig. 9a, close to the origin.

Our numerical results show that the steady-state (63) with $p^B = 0$ is realizable from the long-time dynamics of the full transport model (90) with different initial states for p^W, p^B, and p^U at $t = 0$. In Fig. 9 we plot the numerical solution p^W and p^U to (90) at $t = 130$ for the parameter values $\varepsilon = 0.02$, $k_b = 0.3$, $k_{bw} = 0.5$, and $D = 0.1$, when the initial densities are spatially uniform and equally partitioned as $p^W = p^B = p^U = 1/3$ at $t = 0$. The full dynamics quickly drives p^B to zero as t increases. From Fig. 9, at $t = 130$ we observe that the computed motor densities p^W and p^U from the full model agree well with the steady-state asymptotic result (63).

4.3.2 Type II Quasi-Steady-States: $p^B > 0$

For our second choice we let $p^B \neq 0$ be the free parameter, and define $p^B = \alpha(x,t)$. Upon solving (57) for p^W and p^U, we obtain the quasi-steady-state solution for (90) given by

$$\mathbf{p}^0(\alpha) = \begin{pmatrix} p^W \\ p^B \\ p^U \end{pmatrix} = \begin{pmatrix} \frac{1}{k_{bw}\alpha} \\ \alpha \\ \frac{1}{k_b}\left(\alpha + \frac{1}{k_{bw}\alpha}\right) \end{pmatrix}. \tag{64}$$

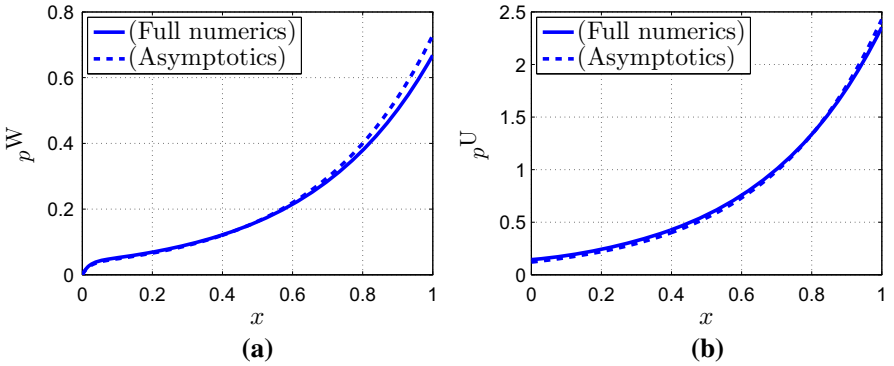

Fig. 9 Full numerical versus asymptotic solutions to the myosin model. Shown are steady-state motor densities (*solid curves*) p^{W} (**a**) and p^{U} (**b**) (shown at $t = 130$) computed from the full time-dependent myosin transport model (90) for $\varepsilon = 0.02$ and with the spatially uniform initial condition $p^{\mathrm{W}} = p^{\mathrm{B}} = p^{\mathrm{U}} = 1/3$ at $t = 0$, so that the total mass is unity. The parameters are $k_{\mathrm{b}} = 0.3$, $k_{\mathrm{bw}} = 0.5$, and $D = 0.1$. Although $p^{\mathrm{B}} > 0$ at $t = 0$, the dynamics quickly drives p^{B} to zero as t increases. The *dashed curves* in **a** and **b** are the asymptotic results (63) for the steady-state, which compare favourably with the numerical results

Next, we calculate the eigenvalues λ of the Jacobian of the kinetics $\mathbf{f}(\mathbf{p})$ at $\mathbf{p} = \mathbf{p}^0$ to determine whether $\mathbf{p}^0$ is a slow manifold in the sense of Definition 3.1. After some algebra we obtain that $\lambda = 0$, while the remaining two eigenvalues $\lambda_\pm$ satisfy the quadratic equation $\lambda^2 - \sigma_1\lambda + \sigma_2 = 0$, where σ_1 and σ_2 are given by

$$\sigma_1 = -2 - k_{\mathrm{b}} + 2k_{\mathrm{bw}}p^{\mathrm{B}}p^{\mathrm{W}} - k_{\mathrm{bw}}\left(p^{\mathrm{B}}\right)^2, \tag{65a}$$

$$\sigma_2 = \left(1 - 2k_{\mathrm{bw}}p^{\mathrm{B}}p^{\mathrm{W}}\right)\left(1 + k_{\mathrm{b}} + k_{\mathrm{bw}}(p^{\mathrm{B}})^2\right) + 2k_{\mathrm{bw}}^2(p^{\mathrm{B}})^3p^{\mathrm{W}} - k_{\mathrm{b}} + k_{\mathrm{b}}\left(1 + k_{\mathrm{bw}}(p^{\mathrm{B}})^2\right), \tag{65b}$$

with p^{B} and p^{W} as given by the entries in (64). Upon using (64) for $\mathbf{p}^0$, we calculate σ_1 and σ_2 to

$$\sigma_1 \equiv -k_{\mathrm{b}} - \alpha^2 k_{\mathrm{bw}}, \qquad \sigma_2 \equiv (k_{\mathrm{b}} + 1)\left(\alpha^2 k_{\mathrm{bw}} - 1\right). \tag{66}$$

Since $\sigma_1 < 0$, a necessary and sufficient condition for $\mathrm{Re}(\lambda_\pm) < 0$ is that $\sigma_2 > 0$ in (66). We conclude from the expression for σ_2 in (66) that $\mathbf{p}^0$ is a slow manifold whenever $k_{\mathrm{bw}} > 1/\alpha^2$.

For $k_{\mathrm{bw}} > 1/\alpha^2$, we derive the QSS PDE by imposing the solvability condition (24a). This yields that

$$(1,1,1)\frac{\partial}{\partial t}\begin{pmatrix} \frac{1}{k_{\mathrm{bw}}\alpha} \\ \alpha \\ \frac{\alpha}{k_{\mathrm{b}}} + \frac{1}{k_{\mathrm{b}}k_{\mathrm{bw}}\alpha} \end{pmatrix} = (1,1,1)\mathbf{M}\begin{pmatrix} \frac{1}{k_{\mathrm{bw}}\alpha} \\ \alpha \\ \frac{\alpha}{k_{\mathrm{b}}} + \frac{1}{k_{\mathrm{b}}k_{\mathrm{bw}}\alpha} \end{pmatrix}. \tag{67}$$

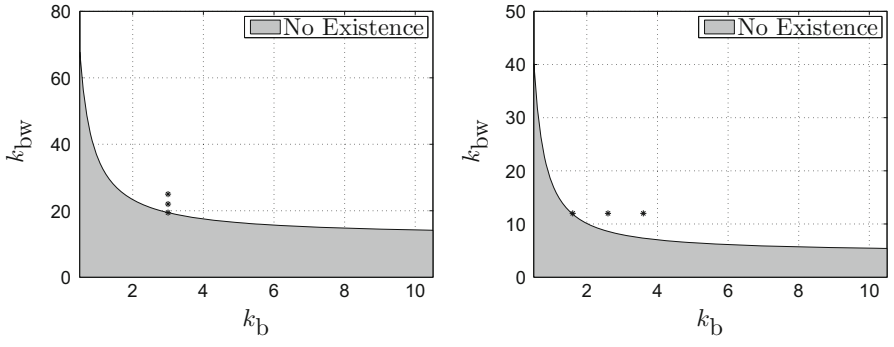

Fig. 10 Region of solution existence (*unshaded*). Shown are the regions in the k_{bw} versus k_b parameter space where a steady-state to the myosin model Type II QSS PDE (68) for $D = 0.1$ exists when **a** $v = 0.1$ and **b** $v = 0.5$. In the *shaded regions*, there is no steady-state to the Type II QSS PDE. On the boundary of these regions $\alpha = 1/\sqrt{k_{bw}}$ at $x = 0$. The total mass was fixed at $\int_0^1 y(x,0)\,dx = 1$. The points marked in the *left* and *right panel* are parameter values where solutions are shown in Figs. 11 and 12, respectively

By calculating the various terms in this expression, we obtain the following nonlinear QSS PDE for $\alpha(x,t)$:

$$\frac{\partial}{\partial t}\left(\frac{(k_b+1)(k_{bw}\alpha^2+1)}{k_b k_{bw}\alpha}\right) = \frac{\partial}{\partial x}\left(\mathscr{V}(\alpha)\alpha + \mathscr{D}(\alpha)\frac{\partial \alpha}{\partial x}\right), \tag{68a}$$

where the "effective transport rate" and the "effective rate of diffusion" are given by

$$\mathscr{V}(\alpha) = v\alpha - \frac{1}{k_{bw}\alpha}, \qquad \mathscr{D}(\alpha) = D\frac{(k_{bw}\alpha^2-1)}{k_b k_{bw}\alpha^2}. \tag{68b}$$

From (108) of "Appendix D", the zero-flux boundary conditions for this conservation law are

$$\mathscr{V} + \mathscr{D}\frac{\partial \alpha}{\partial x} = 0, \qquad \text{at} \quad x = 0, 1, \tag{68c}$$

which are exactly zero-flux boundary conditions for the QSS PDE (68). From (68b) we observe that the advection direction depends on the sign of $\mathscr{V}$. In particular, if $\alpha < 1/(\sqrt{vk_{bw}})$, the net movement is to the right. By integrating the QSS PDE over the domain, and by using (68c), we obtain a conservation law for $y(x,t) = \mathbf{e}^T\mathbf{p}^0[\alpha(x,t)]$, where $\mathbf{p}^0(\alpha)$ is defined in (64). For all $t > 0$, we obtain in terms of $\alpha(x,t)$ that

$$\int_0^1 y(x,t)\mathrm{d}x = \int_0^1 y(x,0)\,\mathrm{d}x, \qquad y(x,t) \equiv \frac{(k_b+1)}{k_b k_{bw}}\frac{(k_{bw}\alpha^2+1)}{\alpha}. \tag{69}$$

We remark that on the range $k_{bw}\alpha^2 - 1 > 0$ for which $\mathbf{p}^0$ is a slow manifold for the dynamics, the QSS PDE (68a) is well-posed in that the diffusion coefficient in

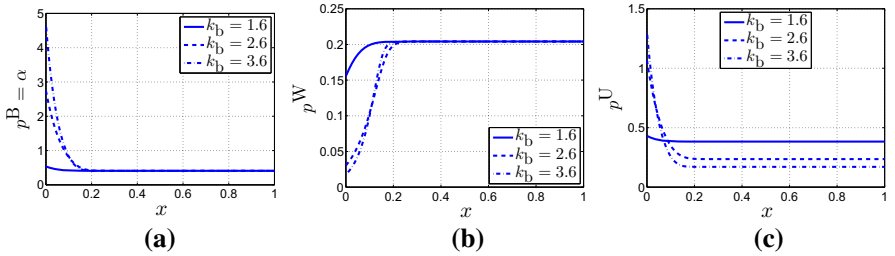

Fig. 11 Effect of the (scaled) binding rate, k_{b}. We show the QSS densities p^{B} (**a**), p^{W} (**b**), and p^{U} (**c**), computed from (71) and (64), for three values of k_{b} corresponding to taking a horizontal slice through the parameter space in Fig. 10b with fixed $k_{\mathrm{bw}} = 12$. Other parameters are $D = 0.1$ and $v = 0.5$. The total mass was fixed at $\int_0^1 y(x)\,\mathrm{d}x = 1$. **a** p^{B} versus x. **b** p^{W} versus x. **c** p^{U} versus x

(68a) is positive. In fact by expanding (68a), we obtain that (68a) is equivalent to the following PDE with a constant diffusivity $D/(k_{\mathrm{b}}+1)$,

$$\frac{\partial \alpha}{\partial t} = \frac{D}{k_{\mathrm{b}}+1}\frac{\partial^2 \alpha}{\partial x^2} + \frac{k_{\mathrm{bw}}k_{\mathrm{b}}}{(k_{\mathrm{b}}+1)(k_{\mathrm{bw}}\alpha^2-1)} \times \left(\left(v\alpha^2 + \frac{1}{k_{\mathrm{bw}}}\right)\frac{\partial \alpha}{\partial x} + \frac{2D}{\alpha k_{\mathrm{b}}k_{\mathrm{bw}}}\left(\frac{\partial \alpha}{\partial x}\right)^2\right). \tag{70}$$

Alongside the transport term involving $\frac{\partial \alpha}{\partial x}$, the source term $\frac{2D}{\alpha k_{\mathrm{b}}k_{\mathrm{bw}}}\left(\frac{\partial \alpha}{\partial x}\right)^2$ describes how gradients in α can lead to an increase in motor density, especially for low densities (so that $1/\alpha$ is large).

Steady-state solutions to the QSS PDE (68) are solutions to the non-local problem

$$\frac{\mathrm{d}\alpha}{\mathrm{d}x} = -\frac{k_{\mathrm{b}}}{D}\frac{\left(vk_{\mathrm{bw}}\alpha^2-1\right)}{k_{\mathrm{bw}}\alpha^2-1}\alpha, \qquad \frac{(k_{\mathrm{b}}+1)}{k_{\mathrm{b}}k_{\mathrm{bw}}}\int_0^1 \frac{(k_{\mathrm{bw}}\alpha^2+1)}{\alpha}\,\mathrm{d}x = 1, \tag{71}$$

provided that $k_{\mathrm{bw}}\alpha^2 - 1 > 0$ on $0 \le x \le 1$. Here we have fixed the total mass as $\int_0^1 y(x,0)\,\mathrm{d}x = 1$. We use the numerical shooting method described in "Appendix C" to solve (71) and, further, to numerically identify the region in the k_{bw} versus k_{b} parameter space where $k_{\mathrm{bw}}\alpha^2 - 1 > 0$ on $0 < x < 1$. For $D = 0.1$, this region is shown in Fig. 10a, b for $v = 0.1$ and $v = 0.5$, respectively.

In Fig. 11a–c we plot the QSS motor densities $p^{\mathrm{B}}(x)$, $p^{\mathrm{W}}(x)$, and $p^{\mathrm{U}}(x)$, for three values of k_{b} corresponding to taking a horizontal slice at fixed $k_{\mathrm{bw}} = 12$ through the parameter plane in Fig. 10b with $v = 0.5$. In terms of $\alpha(x)$, these densities are given by (64). From Fig. 11a–b we observe that as k_{b} increases there is an accumulation of bound myosin motors, with a corresponding decrease in walking myosin motors near the left end of the cell. From Fig. 11c we observe that as k_{b} increases, there is a decrease in unbound freely diffusing motors in the cytosolic compartment in the middle of the cell.

In Fig. 12a–c we plot the QSS motor densities $p^{\mathrm{B}}(x)$, $p^{\mathrm{W}}(x)$, and $p^{\mathrm{U}}(x)$, for three values of k_{bw} corresponding to taking a vertical slice at fixed $k_{\mathrm{b}} = 3.0$ through the

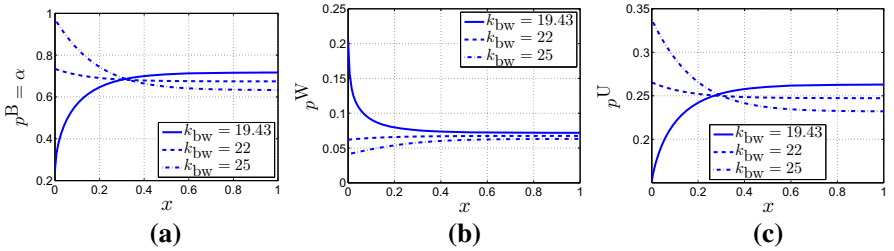

Fig. 12 Effect of the (scaled) stalling rate, k_{bw}. As in Fig. 11 but for three values of k_{bw} corresponding to taking a vertical slice through the parameter space in Fig. 10a with fixed $k_{\mathrm{b}} = 3.0$. **a** p^{B} versus x. **b** p^{W} versus x. **c** p^{U} versus x

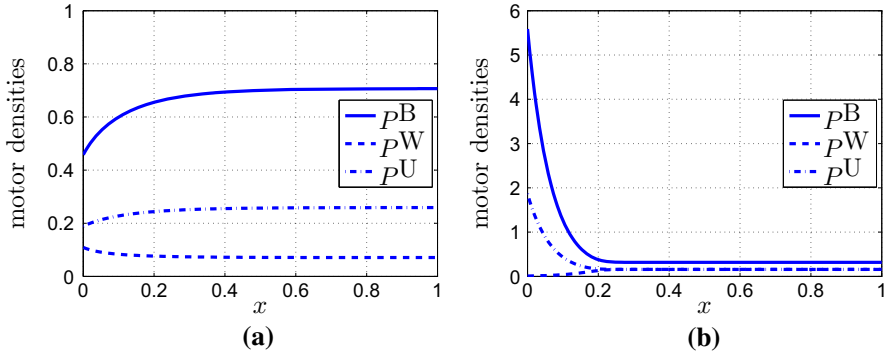

Fig. 13 Effect of treadmilling speed, v, QSS densities p^{B}, p^{W}, and p^{U}, computed from (71) and (64), for **a** $v = 0.1$ and **b** $v = 0.5$. As v increases, we observe that the system switches from right-biased advection to left-biased advection. Other parameters are $k_{\mathrm{bw}} = 20$, $k_{\mathrm{b}} = 3$, and $D = 0.1$. The total mass is $\int_0^1 y(x, 0)\,\mathrm{d}x = 1$

phase-diagram in Fig. 10a with $v = 0.1$. We observe from Fig. 12a, b that as the transition rate k_{bw} between walking to bound motors increases, there is a decrease in walking motors, with a corresponding increase in bound motors near the left end of the cell.

Finally, in Fig. 13a, b we plot the QSS motor densities for $v = 0.1$ and $v = 0.5$, respectively, for the parameters $k_{\mathrm{b}} = 3$, $k_{\mathrm{bw}} = 20$, and $D = 0.1$. As the treadmilling speed, v, increases from $v = 0.1$ to $v = 0.5$, we observe that the system switches from right-biased advection to left-biased advection. This matches the observation that net movement is to the right if $p^{\mathrm{B}} \equiv \alpha < 1/\sqrt{vk_{\mathrm{bw}}}$. For small treadmilling velocity v, this condition is more easily satisfied since the quantity $1/\sqrt{vk_{\mathrm{bw}}}$ is large.

Two notable features distinguish the myosin model from previous models discussed in this paper. The first is existence of two possible QSS approximations, as we have shown. A second feature pertains to the boundary layer behaviour near $x = 0$ and $x = 1$. This is analysed in detail in "Appendix D.3" based on the full myosin transport model (90) near $x = 0$. There we show, using phase-plane analysis, that we can always insert a boundary layer near $x = 0$ to satisfy $p^{\mathrm{W}} = 0$ at $x = 0$. However, "Appendix D.3" shows that there is no steady-state boundary layer solu-

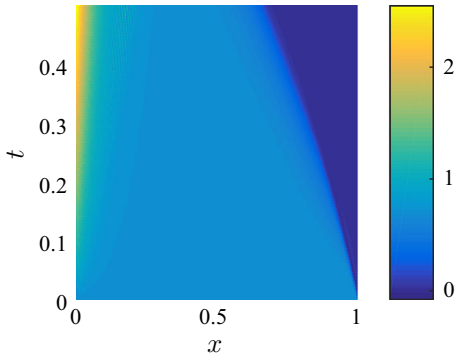

Fig. 14 $p^{\mathrm{B}}(x,t)$ converges to Type I QSS. The density of bound motors, $p^{\mathrm{B}}(x,t)$, tends to zero behind a wave propagating backwards from $x=1$. The full myosin model converges to a Type I QSS as no non-trivial steady-state solution satisfies the boundary condition $p^{\mathrm{B}}(1)=0$. Parameters are $k_{\mathrm{bw}}=25$, $k_{\mathrm{b}}=3$, $D=0.1$, $v=0.5$, and $\varepsilon=0.02$ (Color figure online)

tion near $x=1$ that allows the extra boundary condition $p^{\mathrm{B}}=0$ at $x=1$ to be satisfied. This difficulty results from the fact that $p^{B}=0$ is the slow manifold for the Type I solutions of Sect. 4.3.1. Since no steady-state boundary layer solution exists in the full model, we find that any nonzero density of stalled motors p^{B} will tend to 0 via a backwards propagating wave that leaves $p^{\mathrm{B}}=0$ in its wake. We find that the full myosin model converges to a Type I QSS (58) regardless of the initial condition. An example of this behaviour is shown in Fig. 14, where $k_{\mathrm{bw}}=25$, $k_{\mathrm{b}}=3$, $D=0.1$, $v=0.5$, and $\varepsilon=0.02$. As a result, drawing conclusions about the behaviour of the full system from the QSS PDE becomes difficult. This leads to the question of which QSS PDE, Type I or Type II, better describes the bulk system dynamics.

One possible regularization to overcome this problem with the boundary layer near $x=1$ is to add an asymptotically small diffusion term $\varepsilon_1 p^{\mathrm{B}}_{xx}$ to (90), where $\varepsilon_1=\mathcal{O}(\varepsilon)$, which to leading-order does not affect the quasi-steady-states. The addition of such a small "regularizing" diffusion term also appears in the travelling wave analysis of Yochelis and Gov (2016). The fully scaled model is as in (90c), but with the additional small diffusion term in the p^{B} equation:

$$\frac{\partial p^{\mathrm{W}}}{\partial t}=-\frac{\partial p^{\mathrm{W}}}{\partial x}+\frac{1}{\varepsilon}\left(-k_{\mathrm{bw}}\left(p^{\mathrm{B}}\right)^{2}p^{\mathrm{W}}+k_{\mathrm{b}}p^{\mathrm{U}}-p^{\mathrm{W}}\right), \tag{72a}$$

$$\frac{\partial p^{\mathrm{B}}}{\partial t}=\varepsilon_1\frac{\partial^2 p^{\mathrm{B}}}{\partial x^2}+v\frac{\partial p^{\mathrm{B}}}{\partial x}+\frac{1}{\varepsilon}\left(k_{\mathrm{bw}}\left(p^{\mathrm{B}}\right)^{2}p^{\mathrm{W}}-p^{\mathrm{B}}\right), \tag{72b}$$

$$\frac{\partial p^{\mathrm{U}}}{\partial t}=D\frac{\partial^2 p^{\mathrm{U}}}{\partial x^2}+\frac{1}{\varepsilon}\left(p^{\mathrm{B}}+p^{\mathrm{W}}-k_{\mathrm{b}}p^{\mathrm{U}}\right). \tag{72c}$$

The boundary conditions are as before, (12) and (13), but instead of $p^{\mathrm{B}}(1,t)=0$, we now impose that

$$\frac{\partial p^{\mathrm{B}}}{\partial x}(0,t)=0 \quad \text{and} \quad \frac{\partial p^{\mathrm{B}}}{\partial x}(1,t)=0, \tag{73}$$

for conservation of mass.

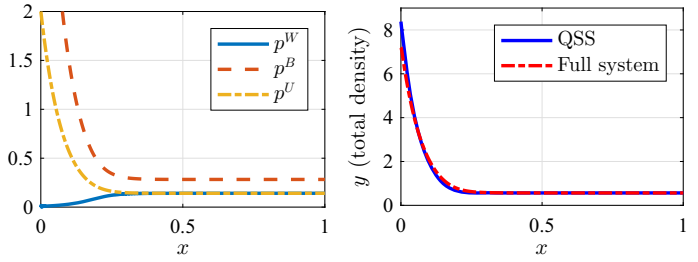

Fig. 15 Steady-state behaviour of the regularized myosin model. **a** The steady-state behaviour of the full myosin model with small p^{B} diffusion term. Note that $p^{\mathrm{B}} > 0$ for all x. **b** A comparison of the total density of myosin in the Type II QSS approximation and in the full model. Note that this Type II QSS behaviour approximates the full system dynamics well. Parameters are $k_{\mathrm{bw}} = 25$, $k_{\mathrm{b}} = 3$, $D = 0.1$, $v = 0.5$, $\varepsilon = 0.02$, and $\varepsilon_1 = 0.005$. The total mass was fixed at $\int_0^1 y(x)\,\mathrm{d}x = 1$ (Color figure online)

In this case, both Type I and Type II QSS PDEs are valid approximations of the full system, and it is possible to add steady-state boundary layers near $x = 0$ and $x = 1$ for the regularized model (72). However, it is intractable analytically to analyse the global behaviour of time-dependent solutions for (72), so as to predict which of the two types of QSS PDEs will result from an arbitrary initial state. In Fig. 15a, we show that the full model (72) with asymptotically small diffusion term $\varepsilon_1 p^{\mathrm{B}}_{xx}$ has a steady-state with nonzero p^{B} and that solutions can converge to the Type II QSS (as compared with Fig. 14). In this case, as shown in Fig. 15b, solutions to the full myosin model and the Type II QSS PDE agree as expected.

Due to the existence of two QSS solutions, we predict that the initial condition for (72) determines whether the full myosin model converges to the Type I or Type II QSS. To elucidate this hypothesis, we fix the model parameters $k_{\mathrm{bw}} = 25$, $k_{\mathrm{b}} = 3$, $D = 0.1$, $v = 0.5$, $\varepsilon = 0.02$, and $\varepsilon_1 = 0.005$ and numerically determine which QSS the regularized full system of PDE's (72) converges to for a range of spatially homogenous initial conditions. We choose spatially homogenous constant initial conditions: $p^{\mathrm{W}}(x, 0) = c_1$, $p^{\mathrm{B}}(x, 0) = c_2$, with $0 \leq c_2, c_2 \leq 1$, $c_1 + c_2 \leq 1$ and $p^{\mathrm{U}}(x, 0) = 1 - c_1 - c_2$ to ensure conservation of total mass. In Fig. 16, the results of this exploration are shown in a phase-diagram. For a given pair of spatially homogenous initial conditions, $(p^{\mathrm{B}}(x, 0), p^{\mathrm{W}}(x, 0))$, a circle indicates that the model (72) converges to a Type I QSS, while a cross indicates that the model (72) converges to a Type II QSS. The line on the phase-diagram indicates the unstable manifold which emanates from a saddle-point steady-state in the myosin model reaction kinetics (the non-spatial myosin model). For a phase-plane analysis of the non-spatial myosin model, see Appendix B.4. Below this unstable manifold, the non-spatial myosin reaction kinetics converge to a steady-state with $p^{\mathrm{B}} = 0$, similar to a Type I QSS. Above this unstable manifold, the non-spatial model converges to a steady-state with $p^{\mathrm{B}} > 0$, similar to a Type II QSS. The discrepancy between the unstable manifold computed from the non-spatial model and the phase-diagram from the fully spatial model indicates that the spatial processes enlarge the region of attraction for Type II QSS with nonzero p^{B}.

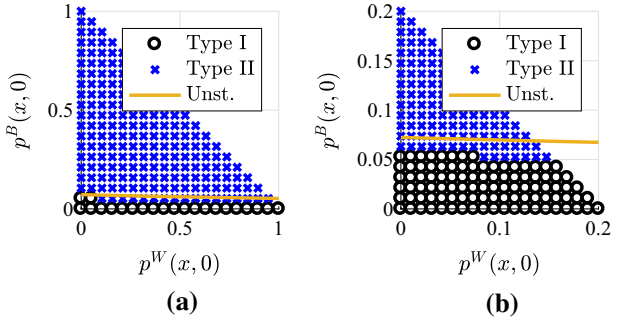

Fig. 16 Myosin model initial condition dependence. The steady-state behaviour of the full myosin model with p^{B} diffusion depends on the initial conditions. For a given pair of spatially homogenous initial conditions, $\left(p^{\mathrm{W}}(x,0), p^{\mathrm{B}}(x,0)\right) = (c_1, c_2)$, with $p^{\mathrm{U}}(x,0) = 1 - c_1 - c_2$, the solution will converge to a Type I steady-state, with $\int_0^1 p^{\mathrm{B}}(x)\,\mathrm{d}x = 0$ (indicated by a *circle*), or to a Type II steady-state (*cross*), with $\int_0^1 p^{\mathrm{B}}(x)\,dx > 0$. The *line* in the phase-diagram represents the unstable manifold computed from the non-spatial myosin model (Sect. B.4). In the non-spatial model, the solution converges to a Type I steady-state ($p^{\mathrm{B}} = 0$) with initial conditions below this unstable manifold, while the solution converges to a Type II steady-state ($p^{\mathrm{B}} > 0$) with initial conditions above this unstable manifold. Parameters are $k_{\mathrm{bw}} = 25$, $k_{\mathrm{b}} = 3$, $D = 0.1$, $v = 0.5$, $\varepsilon = 0.02$, and $\varepsilon_1 = 0.005$. The total mass was fixed at $\int_0^1 y(x)\,\mathrm{d}x = 1$. **a** Phase-diagram, **b** enlarged version of **a**

5 Discussion

The quasi-steady-state reduction method for molecular motor transport was introduced in Newby and Bressloff (2010b) for reaction–advection–diffusion systems with linear reaction kinetics. Here we have generalized this method to a class of problems where the kinetics are nonlinear, but where a conservation condition is satisfied. The QSS method relies on the assumption that the nonlinear kinetics occur on a faster timescale than the diffusion and advection processes. In this limit of fast reaction kinetics, and under a condition on the eigenvalues of the Jacobian of the kinetics, the full system dynamics were shown to be well approximated by the dynamics on a slow solution manifold, which consists of a single scalar quasi-steady-state PDE. This asymptotic formalism was used to analyse three specific nonlinear models for the binding and unbinding of molecular motors.

The models we used as case studies included the following: (1) a model with nonlinearity in the binding rate of motors to MT (due to saturation, with and without binding cooperativity). This model reduces (with parameter $c = 0$) to the linear binding case considered in a previous study (Dauvergne and Edelstein-Keshet 2015) and is used here as a basic "control" to validate our method. Typical biochemical binding functions, such as Michaelis–Menten or Hill function kinetics were used to describe the dependence of binding rate on the free motor density (represented by the increasing and saturating function g). Here the nonlinearity was a function of a single state variable. (2) In the second class of models, nonlinearity stemmed from interaction between motors in different states, such as collisions that lead to direction changes or stalling while bound to a MT. Both

the kinesin–dynein complex model and the myosin motor model shared such aspects.

Each model we explored satisfied a conservation law, namely that the total density of motors was fixed in the cell. This constraint served an important purpose, as it was used to reduce the system from n to $n-1$ states (where $n=3$ for all our models). In each case, we defined the population of motors in various states in terms of one reference state [denoted by $\alpha(x)$]. The choice for that reference state was merely a matter of convenience of calculations and was not the same for all cases.

We found that many elements of the linear QSS theory carry over. However, the geometry of projections in the linear case [as developed in Newby and Bressloff (2010b), Bressloff and Newby (2013)] no longer holds, which suggests that obtaining higher-order terms in asymptotic solutions is no longer tractable. Obtaining expressions for such correction terms remains an open problem. Moreover, in many cases, the diffusion coefficient in the unbound state is taken to be $\mathcal{O}(\varepsilon)$. If this is the case, in those particular cases where the drift term vanishes, our QSS PDE would simply reduce to a conservation law for the total density of motors in the system and fail to describe the dynamics of the system. To avoid this, we take the diffusion coefficient in the unbound state to be $\mathcal{O}(1)$.

For all such models, our QSS reduction of (15) leads to new scalar nonlinear PDEs, which do not seem to be amenable to analytical solution techniques. Although we were still required to solve these QSS PDEs numerically, the QSS reduction does effectively eliminate the small parameter ε from the full model and avoids the more challenging numerical task of having to compute solutions to the full nonlinear vector system (15) of PDEs at each small ε.

The QSS analysis allows us to draw conclusions about the overall rate of transport (advection velocity) of the system that results from the combination of motors walking on MT, diffusing while unbound, and kinetics of binding, unbinding, switching directions, and/or stalling. Additionally, the QSS PDE was shown to readily allow insight into the behaviour of the steady-state solutions as parameters are varied. This insight was used to interpret cell-level behaviours resulting from various specific mathematical models of motor interactions. We summarize some of our major conclusions and their implications below for each of the case studies.

Kinesin Model Here the cytosolic motor state was used as the reference state α, and a Fokker–Planck (FP) equation (29) was derived for the total motor density. In the special case of spatially constant MT bias, this reduced further to the FP equation (33a) for the cytosolic state from which we can draw several conclusions. (a) The overall transport direction depends on the sign of $(1-2P)$. (b) When $(1-2P)\neq 0$ (which means that more MTs point to one end of the cell than to the other) we predict an exponential spatial motor distribution, whose maximum coincides with the cell end to which MTs are biased. (c) Both the effective diffusion and the effective transport rates are (essentially) averages of the diffusion and transport rates in the underlying states, weighted by the fraction of time spent in each of those states. These conclusions are consistent with results of the linear models in Dauvergne and Edelstein-Keshet (2015). (d) When MT polarity bias $P(x)$ is spatially non-uniform, there arises the possibility for motors to pile up either at cell ends or in the middle of the cell, as shown in Fig. 5.

This reflects the earlier results for the QSS reduction of a model with spatially varying parameters. In this case, the resulting QSS PDE had spatially dependent effective diffusion and velocity (Newby and Bressloff 2010a). (e) The overall effect of nonlinear binding in this case is that more kinesin motors are sequestered in the freely diffusing class, which results in a shallower motor density across the cell. The shallower solution profile results from the fact that the binding rate is limited in both the saturated binding and Hill function binding cases. (f) Hill function binding (which could represent cooperative motor binding interactions) creates "kinks" and inflection points in the spatial motor distribution, since the Hill function turns binding on or off more sharply than does Michaelis–Menten kinetics.

Kinesin–Dynein Model Here the nonlinearity involves a product of two state variables (left- and right-moving complexes), a composite left–right bias function $Q(x)$, and possibly distinct velocities when moving right or left. (See "Appendix A.2" for the relationship of the function Q to the underlying biological details.) Here the left-moving motor variable was used as reference state α. We found that both effective transport rate and effective diffusion rate are "density dependent" (functions of α). The effective transport rate depends intuitively on the model parameters. Increasing the velocity of left-moving complexes, decreasing the probability of binding to the right-moving state, or increasing the right-to-left turning rate all results in biasing transport towards the left end of the cell. The effective diffusion rate is scaled by $1/k_{\mathrm{a}}$, the association constant, which intuitively modulates how many molecular motor complexes remain in the cytosolic vs. bound states. The effective diffusion rate is further increased from baseline through the "tug-of-war" that the motor complex exerts on its cargo. This increase results from the product $(1-Q)Q$, which gives the probability of binding into the left-moving and right-moving state. Although a motor cannot simultaneously bind into the left-moving and right-moving state, we find that the competition between right-moving and left-moving states increases the effective diffusion of the system—this makes sense, as any rapid switching between right- and left-moving states is similar to a diffusive mechanism.

Myosin Model The motor interference was assumed to cause stalling with a higher-degree nonlinearity ($(p^{\mathrm{B}})^2 p^{\mathrm{W}}$) than in the kinesin–dynein motor complex model, which was inspired by the nonlinear interactions in a model for myosin aggregations (Yochelis and Gov 2016; Yochelis et al. 2015). Moreover, the stalled and walking myosin motors have different velocities, with the stalled motors being transported due to actin treadmilling. Interestingly, this higher-degree nonlinearity gave rise to two distinct QSS solutions, one of which was characterized by the absence of stalled motors ($p^B = 0$, "Type I QSS"). In this case, the QSS PDE is linear and the steady-state solution can be found explicitly. For the second QSS solution with $p^B \neq 0$, we identified a nonlinear FP equation with diffusivity $D/(1+k_{\mathrm{b}})$, a density-dependent effective transport term, and an additional term proportional to $(\partial\alpha/\partial x)^2$. We showed that the latter ("Type II QSS") exists only for a subset of parameters (Fig. 10). Moreover, solutions to the full system converge to the Type I solution, unless the model is corrected by an asymptotically small diffusion term for the stalled motors. Interestingly, such a term had been included in the model in Yochelis and Gov (2016). There,

it was justified physically as a small random motion of stalled motors. Our analysis reveals a mathematical justification as well. We showed that this peculiar effect stems from an issue with the boundary layer at the cell end $x = 1$. The small diffusive correction term changes the p^{B} equation from hyperbolic to parabolic, allowing the model to be consistent with boundary conditions that the uncorrected model cannot satisfy. In this case, the existence of two QSS solutions required further investigation of the behaviour of the full myosin model. We used extensive numerical simulations to determine which QSS PDE would better describe the dynamics of the full system (Fig. 16). In the end, a phase-plane analysis of the non-spatial kinetic model can largely suggest which QSS PDE would be valid for which set of spatially homogenous initial conditions.

All in all, we showed the extent to which QSS analysis is generalizable to nonlinear models for molecular motors. That said, we recognize that all examples discussed herein are simplified prototypes and caricatures of actual molecular motor behaviour. For example, a caveat of the kinesin model (3) is that the nonlinear binding function, $g(p^{\mathrm{U}})$, may not accurately describe biological effects such as competition for binding sites on a single MT. As formulated with a saturating function for $g(p^{\mathrm{U}})$, the model implies that crowding in some region of the cell is responsible for limiting the binding rate of motors to MTs. We interpret the saturated binding rate as a result of competition or crowding for binding sites on a single MT.

In reality, we know that many more states and interactions between states could occur, making the biological system more interesting, but also much more complicated to analyse mathematically. We have not considered the cases of heterogenous multi-motor complexes composed of a distribution of motor types, nor the additional interactions with cargo such as vesicles or early endosomes. It remains unclear at present whether similar methods would lead to insights into such realistic and complex models. The QSS methodology has also been extended to two-dimensional models in the context of a searcher alternating between ballistic and diffusive movement phases (Bressloff and Newby 2011) with linear kinetics. The method presented here should extend to two-dimensional nonlinear models, provided that the conditions on the kinetic terms are met, although it remains an open problem for which classes of nonlinear kinetics and in which dimensions it is possible to analytically write down an approximating QSS PDE.

Acknowledgements M. J. W. was supported by the NSERC Discovery Grant 81541. L. E. K. was supported by an NSERC Discovery Grant 41870. C. Z. was supported by the NSERC Discovery Grant to L. E. K. and T. S. was supported by a USRA position funded by an NSERC Discovery Grant to L. E. K.

Appendix A: Microtubule Density and Binding by Motor Complexes

A.1 Kinesin Model with Non-uniform MT Density

To explicitly incorporate the possibility that MT density, $m(x)$ (as well as fraction of MT pointing to the right, $P(x)$) varies across the cell, we can write the kinesin model equations as

$$\frac{\partial p^{\mathrm{R}}}{\partial t} = -v\frac{\partial p^{\mathrm{R}}}{\partial x} + P(x)k_{\mathrm{bm}}m(x)g(p^{\mathrm{U}}) - k_{\mathrm{u}}p^{\mathrm{R}}, \tag{74a}$$

$$\frac{\partial p^{\mathrm{L}}}{\partial t} = v\frac{\partial p^{\mathrm{L}}}{\partial x} + (1 - P(x))k_{\mathrm{bm}}m(x)g(p^{\mathrm{U}}) - k_{\mathrm{u}}p^{\mathrm{L}}, \tag{74b}$$

$$\frac{\partial p^{\mathrm{U}}}{\partial t} = D_0\frac{\partial^2 p^{\mathrm{U}}}{\partial x^2} - k_{\mathrm{bm}}m(x)g(p^{\mathrm{U}}) + k_{\mathrm{u}}p^{\mathrm{R}} + k_{\mathrm{u}}p^{\mathrm{L}}. \tag{74c}$$

This modification of the model introduces another factor into coefficients that are already spatially dependent, but otherwise leaves the model structure unchanged. Hence, the techniques in the paper apply as before with $k_{\mathrm{bm}}m(x)$ replacing the parameter k_{b}.

For the purposes of our proof-of-concept analysis, we now restrict attention to uniform MT density so that $m(x) \equiv m_0$ is a constant. Then the model for kinesin is given by (75) as below, with the assignment

$$k_{\mathrm{b}} = k_{\mathrm{bm}}m_0.$$

That is, the binding constant k_{b} is understood to represent the net rate of binding, which includes both the per-MT-binding rate and the MT density.

A.2 Kinesin–Dynein Model and the Function $Q(x)$

The kinesin–dynein model simplifies the binding of free motor complexes into states that move right with probability $Q(x)$ and left with probability $1 - Q(x)$. We consider the case of motor complexes that all have n_k kinesin and n_d dynein components. (The case of complexes with a variety of motor numbers can be handled by considering the mean composition of a complex or the mean ratio between the two motor types.) Let us also define the parameters k_{bd} and k_{bk} as the binding rates for a (single) dynein and for a (single) kinesin to a MT, and consider $m(x)$ as the local MT density. Then we can decompose the quantity $k_{\mathrm{b}}Q$ in the model as follows:

$$k_{\mathrm{b}}Q(x) = m(x)\left[P(x)n_k k_{bk} + (1 - P(x))n_d k_{bd}\right].$$

This related the aggregate binding rate to the probability that a kinesin binds to right-pointing MT and that dynein binds to left-pointing MT. Similarly,

$$k_{\mathrm{b}}(1 - Q(x)) = m(x)\left[(1 - P(x))n_k k_{bk} + P(x)n_d k_{bd}\right].$$

Since such details merely substitute one spatially dependent function for another, the analysis we have described carries over as before.

Appendix B: Scaling the Models and the QSS Reduction

B.1 The Kinesin Model

We consider the kinesin model with uniform MT density and demonstrate its scaling here. This system is

$$\frac{\partial p^{\mathrm{R}}}{\partial t} = -v\frac{\partial p^{\mathrm{R}}}{\partial x} + Pk_{\mathrm{b}}g(p^{\mathrm{U}}) - k_{\mathrm{u}}p^{\mathrm{R}}, \tag{75a}$$

$$\frac{\partial p^{\mathrm{L}}}{\partial t} = v\frac{\partial p^{\mathrm{L}}}{\partial x} + (1-P)k_{\mathrm{b}}g(p^{\mathrm{U}}) - k_{\mathrm{u}}p^{\mathrm{L}}, \tag{75b}$$

$$\frac{\partial p^{\mathrm{U}}}{\partial t} = D_0\frac{\partial^2 p^{\mathrm{U}}}{\partial x^2} - k_{\mathrm{b}}g(p^{\mathrm{U}}) + k_{\mathrm{u}}p^{\mathrm{R}} + k_{\mathrm{u}}p^{\mathrm{L}}. \tag{75c}$$

We define T by

$$T \equiv \int_0^{L_0} \left(p^{\mathrm{R}}(x) + p^{\mathrm{L}}(x) + p^{\mathrm{U}}(x)\right) \mathrm{d}x \equiv \int_0^{L_0} y(x)\,\mathrm{d}x.$$

Then T is the total amount of motors inside the cell, and $\rho = T/L_0$ is the average density of motors in the cell.

Scale space, time, and densities as follows:

$$x^\star = \frac{x}{L_0}, \quad t^\star = \frac{tv}{L_0}, \quad p^{J\star} = \frac{p^J}{\rho}, \quad y^\star = \frac{y}{\rho},$$

where $y^\star = p^{\mathrm{R}\star} + p^{\mathrm{L}\star} + p^{\mathrm{U}\star}$ is the total scaled density. We have scaled distance by the cell length and time by the time that a motor takes to walk across the cell. The densities of each state are scaled by the average motor density across the cell.

Then we can recast the total amount as

$$T = \int_0^1 \left(\rho p^{\mathrm{R}\star}(x^\star) + \rho p^{\mathrm{L}\star}(x^\star) + \rho p^{\mathrm{U}\star}(x^\star)\right) d(L_0 x^\star).$$

Taking out the constant factor of $\rho L_0 \equiv T$ from the integral results in

$$T = \rho L_0 \int_0^1 \left(p^{\mathrm{R}\star}(x^\star) + p^{\mathrm{L}\star}(x^\star) + p^{\mathrm{U}\star}(x^\star)\right) \mathrm{d}x^\star,$$

which leads to

$$\int_0^1 y^\star \mathrm{d}x^\star = \int_0^1 \left(p^{\mathrm{R}\star}(x^\star) + p^{\mathrm{L}\star}(x^\star) + p^{\mathrm{U}\star}(x^\star)\right) \mathrm{d}x^\star = 1.$$

With this scaling, the integral of the total scaled density is unity, which we assume throughout our numerical computations.

Substituting the scaled variables into the PDE system (75) leads to

$$\frac{v}{L_0}\frac{\partial(\rho p^{\mathrm{R}\star})}{\partial t^\star} = \frac{-v}{L_0}\frac{\partial(\rho p^{\mathrm{R}\star})}{\partial x^\star} + k_{\mathrm{u}}\left(P(x)\frac{k_{\mathrm{b}}}{k_{\mathrm{u}}}g(\rho p^{\mathrm{U}\star}) - (\rho p^{\mathrm{R}\star})\right), \tag{76a}$$

$$\frac{v}{L_0}\frac{\partial(\rho p^{\mathrm{L}\star})}{\partial t^\star} = \frac{v}{L_0}\frac{\partial(\rho p^{\mathrm{L}\star})}{\partial x^\star} + k_{\mathrm{u}}\left((1-P(x))\frac{k_{\mathrm{b}}}{k_{\mathrm{u}}}g(\rho p^{\mathrm{U}\star}) - (\rho p^{\mathrm{L}\star})\right), \tag{76b}$$

$$\frac{v}{L_0}\frac{\partial(\rho p^{\mathrm{U}\star})}{\partial t^\star} = \frac{D_0}{L_0^2}\frac{\partial^2(\rho p^{\mathrm{U}\star})}{\partial x^{\star 2}} + k_{\mathrm{u}}\left(\rho p^{\mathrm{R}\star} + \rho p^{\mathrm{L}\star} - \frac{k_{\mathrm{b}}}{k_{\mathrm{u}}}g(\rho p^{\mathrm{U}\star})\right). \tag{76c}$$

Then we can consider two cases, depending on whether the function g is linear or not.
Case I: g **is linear** In this case, we can eliminate the factor ρ from every term. Dividing each term in the equations by $v\rho/L_0$ and dropping the stars leads to

$$\frac{\partial p^{\mathrm{R}}}{\partial t} = -\frac{\partial p^{\mathrm{R}}}{\partial x} + \frac{1}{\varepsilon}\left(P(x)k_{\mathrm{a}}p^{\mathrm{U}} - p^{\mathrm{R}}\right), \tag{77a}$$

$$\frac{\partial p^{\mathrm{L}}}{\partial t} = \frac{\partial p^{\mathrm{L}}}{\partial x} + \frac{1}{\varepsilon}\left((1-P(x))k_{\mathrm{a}}p^{\mathrm{U}} - p^{\mathrm{L}}\right), \tag{77b}$$

$$\frac{\partial p^{\mathrm{U}}}{\partial t} = D\frac{\partial^2 p^{\mathrm{U}}}{\partial x^2} + \frac{1}{\varepsilon}\left(p^{\mathrm{R}} + p^{\mathrm{L}} - k_{\mathrm{a}}p^{\mathrm{U}}\right), \tag{77c}$$

where D, ε, and k_{a} are defined by

$$D \equiv \frac{D_0}{vL_0}, \qquad \varepsilon \equiv \frac{v}{L_0k_{\mathrm{u}}}, \qquad k_{\mathrm{a}} \equiv \frac{k_{\mathrm{b}}}{k_{\mathrm{u}}}. \tag{78}$$

In this case, these dimensionless parameters represent, respectively, the ratio of (time to be transported:time to diffuse) across the cell (D), the ratio of (time spent unbound:time to walk) across the cell (ε), and the ratio of (time spent unbound:time spent bound) (k_{a}).
Case II: g **is Michaelian or Hill**

$$g(p) = g_{\mathrm{m}}\frac{p^n}{K^n + p^n}, \quad n = 1, 2, \ldots.$$

Then, (76) becomes

$$\frac{v}{L_0}\frac{\partial(\rho p^{\mathrm{R}\star})}{\partial t^\star} = \frac{-v}{L_0}\frac{\partial(\rho p^{\mathrm{R}\star})}{\partial x^\star} + k_{\mathrm{u}}\left(P(x)\frac{k_{\mathrm{b}}}{k_{\mathrm{u}}}\frac{g_{\mathrm{m}}(\rho p^{\mathrm{U}\star})^n}{[K^n + (\rho p^{\mathrm{U}\star})^n]} - (\rho p^{\mathrm{R}\star})\right), \tag{79a}$$

$$\frac{v}{L_0}\frac{\partial(\rho p^{\mathrm{L}\star})}{\partial t^\star} = \frac{v}{L_0}\frac{\partial(\rho p^{\mathrm{L}\star})}{\partial x^\star} + k_{\mathrm{u}}\left((1-P(x))\frac{k_{\mathrm{b}}}{k_{\mathrm{u}}}\frac{g_{\mathrm{m}}(\rho p^{\mathrm{U}\star})^n}{[K^n + (\rho p^{\mathrm{U}\star})^n]} - (\rho p^{\mathrm{L}\star})\right), \tag{79b}$$

$$\frac{v}{L_0}\frac{\partial(\rho p^{\mathrm{U}\star})}{\partial t^\star} = \frac{D_0}{L_0^2}\frac{\partial^2(\rho p^{\mathrm{U}\star})}{\partial x^{\star 2}} + k_{\mathrm{u}}\left(\rho p^{\mathrm{R}\star} + \rho p^{\mathrm{L}\star} - \frac{k_{\mathrm{b}}}{k_{\mathrm{u}}}\frac{g_{\mathrm{m}}(\rho p^{\mathrm{U}\star})^n}{[K^n + (\rho p^{\mathrm{U}\star})^n]}\right). \tag{79c}$$

Define a new constant $A \equiv K/\rho$. This constant is the ratio of the motor concentration at which the binding rate is half-maximal to the average motor density in the cell. Divide numerator and denominator of the Hill function by ρ^n. Further, divide every term in the equations by $v\rho/L_0$ as before. Then we obtain after rearranging and dropping the starred notation is

$$\frac{\partial p^{\mathrm{R}}}{\partial t} = -\frac{\partial p^{\mathrm{R}}}{\partial x} + \frac{1}{\varepsilon}\left(P(x)k_{\mathrm{a}}\frac{(p^{\mathrm{U}})^n}{[A^n + (p^{\mathrm{U}})^n]} - p^{\mathrm{R}}\right), \tag{80a}$$

$$\frac{\partial p^{\mathrm{L}}}{\partial t} = \frac{\partial p^{\mathrm{L}}}{\partial x} + \frac{1}{\varepsilon}\left((1-P(x))k_{\mathrm{a}}\frac{(p^{\mathrm{U}})^n}{[A^n + (p^{\mathrm{U}})^n]} - p^{\mathrm{L}}\right), \tag{80b}$$

$$\frac{\partial p^{\mathrm{U}}}{\partial t} = D\frac{\partial^2 p^{\mathrm{U}}}{\partial x^2} + \frac{1}{\varepsilon}\left(p^{\mathrm{R}} + p^{\mathrm{L}} - k_{\mathrm{a}}\frac{(p^{\mathrm{U}})^n}{[A^n + (p^{\mathrm{U}})^n]}\right), \tag{80c}$$

where D and ε are as before, but k_{a} now depends on whether g is a Michaelis–Menten or a Hill function. This holds for any Hill coefficient n. Note that, in particular, for the case $n = 1$, which is the Michaelian case considered, we have that

$$\frac{\partial p^{\mathrm{R}}}{\partial t} = -\frac{\partial p^{\mathrm{R}}}{\partial x} + \frac{1}{\varepsilon}\left(P(x)k_{\mathrm{a}}\frac{p^{\mathrm{U}}}{[1 + cp^{\mathrm{U}}]} - p^{\mathrm{R}}\right), \tag{81a}$$

$$\frac{\partial p^{\mathrm{L}}}{\partial t} = \frac{\partial p^{\mathrm{L}}}{\partial x} + \frac{1}{\varepsilon}\left((1-P(x))k_{\mathrm{a}}\frac{p^{\mathrm{U}}}{[1 + cp^{\mathrm{U}}]} - p^{\mathrm{L}}\right), \tag{81b}$$

$$\frac{\partial p^{\mathrm{U}}}{\partial t} = D\frac{\partial^2 p^{\mathrm{U}}}{\partial x^2} + \frac{1}{\varepsilon}\left(p^{\mathrm{R}} + p^{\mathrm{L}} - k_{\mathrm{a}}\frac{p^{\mathrm{U}}}{[1 + cp^{\mathrm{U}}]}\right), \tag{81c}$$

where $c \equiv 1/A = \rho/K$. In (80) and (81) k_{a} is defined by

$$k_{\mathrm{a}} \equiv \frac{k_{\mathrm{b}}g_{\mathrm{m}}}{k_{\mathrm{u}}\rho} \quad \text{(Hill)}, \qquad k_{\mathrm{a}} \equiv \frac{k_{\mathrm{b}}g_{\mathrm{m}}}{k_{\mathrm{u}}K}, \quad \text{(Michaelis–Menten)}. \tag{82}$$

In either case, the parameter k_{a} describes the ratio of time spent bound to the time spent unbound, mediated by the nonlinear binding kinetics.

Finally, we scale the boundary conditions in (5) to get

$$\left(p^{\mathrm{R}} - p^{\mathrm{L}} - D\frac{\partial p^{\mathrm{U}}}{\partial x}\right)\Big|_{x=0,1} = 0, \tag{83}$$

together with

$$p^{\mathrm{R}}(0,t) = 0 \qquad \text{and} \qquad p^{\mathrm{L}}(1,t) = 0. \tag{84}$$

B.2 Kinesin–Dynein Model Scaling

Define $k_c \equiv k_{rl} - k_{lr}$. Then the model can be written as

$$\frac{\partial p^R}{\partial t} = -v_r \frac{\partial p^R}{\partial x} + k_b Q p^U - k_u p^R - k_c p^R p^L, \tag{85a}$$

$$\frac{\partial p^L}{\partial t} = v_l \frac{\partial p^L}{\partial x} + k_b (1-Q) p^U - k_u p^L + k_c p^R p^L, \tag{85b}$$

$$\frac{\partial p^U}{\partial t} = D_0 \frac{\partial^2 p^U}{\partial x^2} - k_b p^U + k_u (p^R + p^L). \tag{85c}$$

Scale all variables as before. Then terms of the form $(k_c/k_u) p^R p^L$ will lead to the form $(k_c/k_u)\rho p^{R\star} \rho p^{L\star}$, so that what remains, after cancelling out a factor of $v_r \rho / L_0$ from every term in each equation, and dropping the starred quantities, is

$$\frac{\partial p^R}{\partial t} = -\frac{\partial p^R}{\partial x} + \frac{1}{\varepsilon}\left(k_a Q p^U - p^R - k p^R p^L\right), \tag{86a}$$

$$\frac{\partial p^L}{\partial t} = v \frac{\partial p^L}{\partial x} + \frac{1}{\varepsilon}\left(k_a (1-Q) p^U - p^L + k p^R p^L\right), \tag{86b}$$

$$\frac{\partial p^U}{\partial t} = D \frac{\partial^2 p^U}{\partial x^2} + \frac{1}{\varepsilon}\left(p^R + p^L - k_a p^U\right), \tag{86c}$$

where the parameters are

$$v \equiv \frac{v_l}{v_r}, \qquad D \equiv \frac{D_0}{v_r L_0}, \qquad \varepsilon \equiv \frac{v_r}{k_u L_0}, \qquad k_a \equiv \frac{k_b}{k_u}, \qquad k \equiv \frac{k_c \rho}{k_u} = \frac{(k_{rl} - k_{lr})\rho}{k_u}. \tag{87}$$

Here ρ is the average density of motors inside the cell. These dimensionless parameters represent, respectively, the (left:right) walking speed ratio (v), the ratio of (time to be transported:time to diffuse) across the cell (D), the ratio of (time spent unbound:time to walk) across the cell (ε), the ratio of (time spent unbound:time spent bound) (k_a), and the turning parameter k, which represents the ratio of (net right–left direction switches:unbinding rate). We comment that the average density of motors ρ enters into the turning rate parameter due to the nonlinearity of the model with respect to the turning of motors when they collide on a MT.

B.2.1 Details of QSS Reduction of Kinesin–Dynein Model

Next, we provide some details of the QSS reduction of the kinesin–dynein model. Upon setting $f_2 = f_3 = 0$ in (49) we get the two equations

$$k p^R p^L = p^L - k_a (1-Q) p^U, \qquad -k_a p^U + p^R + p^L = 0. \tag{88}$$

It is convenient to let p^{L} be the free variable and parameterize the quasi-steady-state in terms of $p^{\mathrm{L}} = \alpha$. By solving (88) for p^{R} and p^{U}, we get the quasi-steady-state solution $\mathbf{p}^0$ as given in (51). We then readily show that the nonzero eigenvalues $\lambda_\pm$ of the Jacobian of the kinetics satisfy the quadratic equation given in (52) and (53). A necessary and sufficient condition for $\mathrm{Re}(\lambda_\pm) < 0$ is that $\sigma_1 < 0$ and $\sigma_2 > 0$ in (53). To establish this result we need some properties of $H(Q)$ defined in (53). We first observe that $H(0) = 1$, so that trivially $\sigma_1 < 0$ and $\sigma_2 > 0$ when $Q = 0$. Then, since $H'(Q) = -(1 + k\alpha)/(1 + k\alpha - Q)^2 < 0$, it follows that $\sigma_1 < 0$ and $\sigma_2 > 0$ on $0 \le Q \le 1$ provided that we can show that $\sigma_1 < 0$ and $\sigma_2 > 0$ when $Q = 1$. These inequalities do hold at $Q = 1$, since by using $H(1) = (k\alpha - 1)/(k\alpha)$ we readily obtain that $\sigma_1 = -1 - k_{\mathrm{a}} - k\alpha$ and $\sigma_2 = k\alpha(1 + k_{\mathrm{a}}) > 0$ when $Q = 1$. This proves that $\mathrm{Re}(\lambda_\pm) < 0$ for any Q in $0 \le Q \le 1$. As a result, $\mathbf{p}^0$ defined in (51) is a slow manifold in the sense of Definition (3.1) for any Q in $0 \le Q \le 1$. Finally, by using $\mathbf{p}^0$ and the operator M, as defined in (49), in the solvability condition (24), we readily derive the QSS PDE model (54).

B.3 Myosin Model Scaling

We carry out similar scaling for the myosin model characterized by

$$\frac{\partial p^{\mathrm{W}}}{\partial t} = -v_{\mathrm{w}}\frac{\partial p^{\mathrm{W}}}{\partial x} - \hat{k}_{\mathrm{bw}}\left(p^{\mathrm{B}}\right)^2 p^{\mathrm{W}} + \hat{k}_{\mathrm{b}}p^{\mathrm{U}} - k_{\mathrm{u}}p^{\mathrm{W}}, \tag{89a}$$

$$\frac{\partial p^{\mathrm{B}}}{\partial t} = v_{\mathrm{b}}\frac{\partial p^{\mathrm{B}}}{\partial x} + \hat{k}_{\mathrm{bw}}\left(p^{\mathrm{B}}\right)^2 p^{\mathrm{W}} - k_{\mathrm{u}}p^{\mathrm{B}}, \tag{89b}$$

$$\frac{\partial p^{\mathrm{U}}}{\partial t} = D_{\mathrm{f}}\frac{\partial^2 p^{\mathrm{U}}}{\partial x^2} - \hat{k}_{\mathrm{b}}p^{\mathrm{U}} + k_{\mathrm{u}}(p^{\mathrm{B}} + p^{\mathrm{W}}). \tag{89c}$$

When we scale variables just as before, the terms $\left(p^{\mathrm{B}}\right)^2 p^{\mathrm{W}}$ will lead to the forms $\left(\rho p^{\mathrm{B}\star}\right)^2 (\rho p^{\mathrm{W}\star})$. This will result in a constant factor ρ^2 that remains after cancelling out ρ from all terms in the equation. As a result, we will obtain, upon dropping the starred quantities,

$$\frac{\partial p^{\mathrm{W}}}{\partial t} = -\frac{\partial p^{\mathrm{W}}}{\partial x} + \frac{1}{\varepsilon}\left(-k_{\mathrm{bw}}\left(p^{\mathrm{B}}\right)^2 p^{\mathrm{W}} + k_{\mathrm{b}}p^{\mathrm{U}} - p^{\mathrm{W}}\right), \tag{90a}$$

$$\frac{\partial p^{\mathrm{B}}}{\partial t} = v\frac{\partial p^{\mathrm{B}}}{\partial x} + \frac{1}{\varepsilon}\left(k_{\mathrm{bw}}\left(p^{\mathrm{B}}\right)^2 p^{\mathrm{W}} - p^{\mathrm{B}}\right), \tag{90b}$$

$$\frac{\partial p^{\mathrm{U}}}{\partial t} = D\frac{\partial^2 p^{\mathrm{U}}}{\partial x^2} + \frac{1}{\varepsilon}\left(p^{\mathrm{B}} + p^{\mathrm{W}} - k_{\mathrm{b}}p^{\mathrm{U}}\right), \tag{90c}$$

where the dimensionless parameters v, D, ε, k_{bw}, and k_{b} are defined by

$$v \equiv \frac{v_{\mathrm{b}}}{v_{\mathrm{w}}}, \qquad D \equiv \frac{D_{\mathrm{f}}}{v_{\mathrm{w}}L_0}, \qquad \varepsilon \equiv \frac{v_{\mathrm{w}}}{k_{\mathrm{u}}L_0}, \qquad k_{\mathrm{bw}} \equiv \frac{\hat{k}_{\mathrm{bw}}\rho^2}{k_{\mathrm{u}}}, \qquad k_{\mathrm{b}} \equiv \frac{\hat{k}_{\mathrm{b}}}{k_{\mathrm{u}}}. \tag{91}$$

Recall that ρ is the average density of motors inside the cell. These dimensionless parameters represent, respectively, the bound:walking motor speed ratio (v), the ratio of (time to be transported:time to diffuse) across the cell (D), the ratio of (time spent unbound:time to walk) across the cell (ε), the interaction parameter k_{bw}, which represents the ratio of (net rate of collisions that result in direction change:unbinding rate), and the ratio of (time spent unbound:time spent bound) (k_{b}). Note that the average density of motors ρ enters into the interaction rate parameter due to the nonlinearity of the model with motor–motor interaction.

B.4 Non-Spatial Myosin Model

In Sect. 4.3, we seek to determine whether the Type I or Type II QSS PDE better approximates the behaviour of the full myosin system. To understand the behaviour, we study the non-spatial myosin model kinetics through a phase-plane analysis, where the advection and diffusive processes in (90) are neglected.

The non-spatial myosin model kinetics are described by the following system of ODEs:

$$\frac{\mathrm{d}p^{\mathrm{W}}}{\mathrm{d}t} = -k_{\mathrm{bw}}\left(p^{\mathrm{B}}\right)^2 p^{\mathrm{W}} + k_{\mathrm{b}}p^{\mathrm{U}} - p^{\mathrm{W}}, \qquad \frac{\mathrm{d}p^{\mathrm{B}}}{\mathrm{d}t} = k_{\mathrm{bw}}\left(p^{\mathrm{B}}\right)^2 p^{\mathrm{W}} - p^{\mathrm{B}},$$
$$\frac{\mathrm{d}p^{\mathrm{U}}}{\mathrm{d}t} = p^{\mathrm{B}} + p^{\mathrm{W}} - k_{\mathrm{b}}p^{\mathrm{U}}, \tag{92}$$

where time has been scaled to remove the ε dependence. Due to conservation of mass, we can write $p^{\mathrm{U}} = 1 - p^{\mathrm{W}} - p^{\mathrm{B}}$. This facilitates the reduction of this system of three equations to a system of two equations:

$$\frac{\mathrm{d}p^{\mathrm{W}}}{\mathrm{d}t} = -k_{\mathrm{bw}}\left(p^{\mathrm{B}}\right)^2 p^{\mathrm{W}} + k_{\mathrm{b}}\left(1 - p^{\mathrm{W}} - p^{\mathrm{B}}\right) - p^{\mathrm{W}}, \tag{93a}$$
$$\frac{\mathrm{d}p^{\mathrm{B}}}{\mathrm{d}t} = k_{\mathrm{bw}}\left(p^{\mathrm{B}}\right)^2 p^{\mathrm{W}} - p^{\mathrm{B}}. \tag{93b}$$

With $k_{\mathrm{bw}} = 25$ and $k_{\mathrm{b}} = 3$, a phase-plane analysis (see Fig. 17) reveals the existence of an unstable manifold which divides the $(p^{\mathrm{W}}, p^{\mathrm{B}})$ plane into two regions. For initial conditions below this unstable manifold, the system converges to a steady-state with $p^{\mathrm{B}} = 0$, but $p^{\mathrm{W}} > 0$, as in Type I QSS. For initial conditions above this unstable manifold, the system converges to a steady-state with $p^{\mathrm{B}} > 0$, as in Type II QSS.

Appendix C: Numerics for the Steady-State of the QSS PDEs

In this appendix we show how to numerically compute the steady-state solution of the QSS PDEs by recasting the non-local problem into an initial boundary value problem (IBVP), which is amenable to a numerical shooting method.

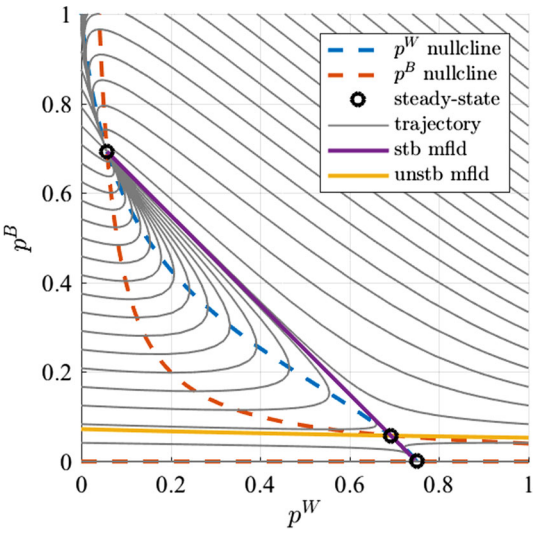

Fig. 17 Phase-plane analysis of the non-spatial myosin model. A phase-plane analysis of the non-spatial myosin model (93) reveals the existence of an unstable manifold that divides $(p^{\mathrm{W}}, p^{\mathrm{B}})$ space into two regions. For initial conditions below the unstable manifold, the system tends to a steady-state with $p^{\mathrm{B}} = 0$, but for initial conditions above the unstable manifold, the system tends to a steady-state with $p^{\mathrm{B}} > 0$ (Color figure online)

For the QSS PDE associated with the **kinesin model** (29) of Sect. 4.1, the steady-state problem is

$$\frac{\mathrm{d}\alpha}{\mathrm{d}x} = \frac{k_{\mathrm{a}}}{D}\left[2P(x) - 1\right] g(\alpha), \qquad \int_0^1 \left(k_{\mathrm{a}} g(\alpha) + \alpha\right) \mathrm{d}x = 1, \tag{94}$$

where $g(\alpha)$ is either the saturated binding model (34) or the Hill function (48). To reformulate (94), we define $N(x)$ by

$$N(x) \equiv \int_0^x \left(k_{\mathrm{a}} g[\alpha(\eta)] + \alpha(\eta)\right) \mathrm{d}\eta - 1. \tag{95}$$

Then, (94) is equivalent to the ODE system

$$\frac{\mathrm{d}\alpha}{\mathrm{d}x} = \frac{k_{\mathrm{a}}}{D}\left[2P(x) - 1\right] g(\alpha), \qquad \frac{\mathrm{d}N}{\mathrm{d}x} = k_{\mathrm{a}} g(\alpha) + \alpha, \tag{96}$$

with $N(0) = -1$. We then specify $\alpha(0) = \beta$, where β is a value to be determined. We solve the IBVPs (96) for various values of β and output the quantity $N(1;\beta)$. In this numerical shooting procedure, Newton's method on β is then used to satisfy the required terminal constraint $N(1;\beta) = 0$.

A similar approach can be used to compute steady-state solutions of the QSS PDE (54) for the **kinesin–dynein model** of Sect. 4.2 subject to the total mass constraint $\int_0^1 y(x)\,\mathrm{d}x = 1$. In place of (96) we obtain

$$\frac{\mathrm{d}\alpha}{\mathrm{d}x} = -\frac{k_\mathrm{a}}{D}\frac{[v(k\alpha+1-Q)-Q]}{(k\alpha+1-Q)^2+Q(1-Q)}(k\alpha+1-Q)\,\alpha,$$
$$\frac{\mathrm{d}N}{\mathrm{d}x} = \left(1+\frac{1}{k_\mathrm{a}}\right)\frac{(k\alpha+1)\alpha}{k\alpha+1-Q}, \tag{97}$$

with $N(0) = -1$ and $\alpha(0) = \beta$, where $\beta > 0$ is a shooting parameter determined numerically by satisfying the terminal constraint $N(1;\beta) = 0$.

Finally, we consider steady-state solutions of the QSS PDE (68) for the **myosin model** of Sect. 4.3 subject to the total mass constraint $\int_0^1 y(x)\,\mathrm{d}x = 1$. In place of (96) we get

$$\frac{\mathrm{d}\alpha}{\mathrm{d}x} = -\frac{k_\mathrm{b}}{D}\frac{\left(vk_\mathrm{bw}\alpha^2-1\right)}{k_\mathrm{bw}\alpha^2-1}\alpha, \qquad \frac{\mathrm{d}N}{\mathrm{d}x} = \frac{(k_\mathrm{b}+1)}{k_\mathrm{b}k_\mathrm{bw}}\frac{(k_\mathrm{bw}\alpha^2+1)}{\alpha}, \tag{98}$$

with $N(0) = -1$ and $\alpha(0) = \beta$, where $\beta > 0$ is computed numerically to satisfy the constraint $N(1;\beta) = 0$. A steady-state solution exists only when $k_\mathrm{bw}\alpha^2 > 1$ on $0 \le x \le 1$.

To numerically determine the boundary in parameter space where $k_\mathrm{bw}\alpha^2 > 1$ holds on $0 \le x \le 1$ for the steady-state when $0 < v < 1$, it is convenient to reformulate (98). We define $A(x) \equiv \sqrt{k_\mathrm{bw}}\alpha(x)$ to transform (98) to

$$\frac{\mathrm{d}A}{\mathrm{d}x} = -c_1\frac{\left(vA^2-1\right)}{A^2-1}A, \qquad \frac{\mathrm{d}N}{\mathrm{d}x} = c_2\frac{\left(A^2+1\right)}{A},$$
$$\text{where} \quad c_1 \equiv \frac{k_\mathrm{b}}{D}, \qquad c_2 \equiv \frac{k_\mathrm{b}+1}{k_\mathrm{b}\sqrt{k_\mathrm{bw}}}. \tag{99}$$

A steady-state solution to the QSS PDE exists only when $A(x) > 1$ on $0 \le x \le 1$. Since (99) implies that $A(x)$ is monotonic in x whenever $A > 1$, then it is possible that $A \to 1^+$ only for $x \to 0^+$ or $x \to 1^-$. However, since $A \to 1/\sqrt{v} > 1$ on the infinite line as $x \to \infty$, it follows that we can only have $A \to 1^+$ as $x \to 0^+$. To determine the local behaviour as $A \to 1^+$ and $x \to 0^+$, we calculate from (99) that $\mathrm{d}A/\mathrm{d}x \sim c_1(1-v)/[2(A-1)]$ and $\mathrm{d}N/\mathrm{d}x \sim 2c_2$. This yields the local behaviour

$$A \sim 1+\sqrt{c_1(1-v)x}, \qquad N \sim -1+2c_2x, \qquad \text{as} \quad x \to 0^+. \tag{100}$$

For a fixed v and $D > 0$, with $0 < v < 1$, to determine the region in the parameter space k_bw versus k_b where $A(x) > 1$ on $0 \le x \le 1$, we proceed as follows. We fix c_1 in (99), numerically integrate the IBVPs (99) with the local behaviour (100) imposed at some $x = \delta$, with $0 < \delta \ll 1$, and numerically shoot on the value of c_2 for which $N(1;c_2) = 0$. From (99), this determines k_b and k_bw as $k_\mathrm{b} = c_1 D$ and $k_\mathrm{bw} = [(k_\mathrm{b}+1)/(k_\mathrm{b}c_2)]^2$.

Appendix D: Boundary Layer Analysis

In this appendix we determine the appropriate boundary conditions for our QSS PDEs, and we analyse the boundary layers near $x = 0, 1$. We focus our discussion on general three-component systems on $0 \le x \le 1$ of the form

$$p_{1t} = -v_1 p_{1x} + \frac{f_1}{\varepsilon}, \qquad p_{2t} = v_2 p_{2x} + \frac{f_2}{\varepsilon}, \qquad p_{3t} = D p_{3xx} + \frac{f_3}{\varepsilon}, \tag{101a}$$

where v_1, v_2, D are positive $\mathcal{O}(1)$ constants, $\varepsilon \ll 1$, and the kinetics $f_j = f_j(p_1, p_2, p_3)$ for $j = 1, \ldots, 3$, satisfy the conservation condition

$$f_1 + f_2 + f_3 = 0. \tag{101b}$$

By imposing the mass constraint $\partial_t \int_0^1 (p_1 + p_2 + p_3)\, dx = 0$, and setting $p_1(0, t) = p_2(1, t) = 0$, we obtain the following boundary conditions for (101a):

$$D p_{3x} + v_2 p_2 - v_1 p_1 = 0, \quad \text{at} \quad x = 0, 1\,; \qquad p_1(0, t) = 0, \quad p_2(1, t) = 0. \tag{101c}$$

We assume that there is a unique one-parameter family $\mathbf{p}^0(\alpha) \equiv (p_1^0(\alpha), p_2^0(\alpha), p_3^0(\alpha))^T$ of solutions to the leading-order problem $\mathbf{f} = (f_1, f_2, f_3)^T = \mathbf{0}$, and that $\mathbf{p}^0$ is a slow manifold for (101) in the sense of Definition 3.1. This is the leading-order outer solution, valid away from boundary layers at $x = 0, 1$. Then, as shown in Sect. 3, $\alpha = \alpha(x, t)$ satisfies the QSS PDE (24a), which can be written as

$$\partial_t \left(p_1^0 + p_2^0 + p_3^0 \right) = \partial_x \left(-v_1 p_1^0 + v_2 p_2^0 + D \partial_x p_3^0 \right). \tag{102}$$

We now determine an appropriate boundary condition for (102) as $x \to 0^+$ by analysing the boundary layer structure for (101) near the left endpoint $x = 0$. As $x \to 0^+$, we obtain from the outer solution that

$$p_1 = p_{10}^0 + \mathcal{O}(x), \qquad p_2 = p_{20}^0 + \mathcal{O}(x), \qquad p_3 \to p_{30}^0 + x \frac{dp_3^0}{dx}\Big|_{x=0} + \cdots, \tag{103}$$

where we have defined $p_{j0}^0 \equiv p_j^0(\alpha(0, t))$ for $j = 1, \ldots, 3$.

We will only analyse in detail the region near $x = 0$, as a similar analysis can be done near $x = 1$. For $t = \mathcal{O}(1)$ the two possible dominant balances for the spatial derivatives in (101a) near $x = 0$ are $x = \mathcal{O}(\sqrt{\varepsilon})$ and $x = \mathcal{O}(\varepsilon)$. On the wider such scale, we let $\xi = x/\sqrt{\varepsilon}$ to obtain from (101a) that

$$p_{1t} = -\frac{v_1}{\sqrt{\varepsilon}} p_{1\xi} + \frac{f_1}{\varepsilon}, \qquad p_{2t} = \frac{v_2}{\sqrt{\varepsilon}} p_{2\xi} + \frac{f_2}{\varepsilon}, \qquad p_{3t} = \frac{D}{\varepsilon} p_{3\xi\xi} + \frac{f_3}{\varepsilon}. \tag{104}$$

To leading-order we obtain that $f_1 = f_2 = 0$, so that from (101b) we must have $f_3 = 0$. As a result, we obtain to leading-order that $p_1 \sim p_{10}^0$, $p_2 \sim p_{20}^0$, and $p_3 \sim p_{30}^0$. This implies that our QSS approximation is still valid when $x = \mathcal{O}(\sqrt{\varepsilon})$.

Next, we analyse the region where $x = \mathcal{O}(\varepsilon)$. Upon introducing $\eta \equiv x/\varepsilon$, we obtain from (101a) that

$$\varepsilon p_{1t} = -v_1 p_{1\eta} + f_1, \qquad \varepsilon p_{2t} = v_2 p_{2\eta} + f_2, \qquad \varepsilon p_{3t} = \frac{D}{\varepsilon} p_{3\eta\eta} + f_3. \tag{105a}$$

From (101c), the boundary conditions for this system are

$$\frac{D}{\varepsilon} p_{3\eta} + v_2 p_2 - v_1 p_1 = 0, \quad \text{at} \quad \eta = 0\,; \qquad p_1(0,t) = 0, \tag{105b}$$

while the asymptotic matching conditions, as obtained from (103), are that

$$p_1 \sim p_{10}^0, \qquad p_2 \sim p_{20}^0, \qquad p_3 \sim p_{30}^0 + \varepsilon\eta \frac{dp_3^0}{dx}\Big|_{x=0}, \qquad \text{as} \quad \eta \to \infty. \tag{105c}$$

For $t = \mathcal{O}(1)$, we neglect the asymptotically negligible left-hand sides of (105a) to obtain

$$-v_1 p_{1\eta} = -f_1, \qquad v_2 p_{2\eta} = -f_2, \qquad \frac{D}{\varepsilon} p_{3\eta\eta} = -f_3. \tag{106}$$

By adding the equations in (106), and using the conservation condition (101b), we obtain upon integration in η that, for all $\eta > 0$,

$$\frac{D}{\varepsilon} p_{3\eta} - v_1 p_1 + v_2 p_2 = A, \tag{107}$$

where A is independent of η. By evaluating this expression at $\eta = 0$, (105b) yields that $A = 0$. With $A = 0$, we then evaluate (107) as $\eta \to \infty$ by using the matching condition (105c). This yields

$$D\frac{\mathrm{d}p_3^0}{\mathrm{d}x} - v_1 p_1^0 + v_2 p_2^0 = 0, \quad \text{at} \quad x = 0. \tag{108a}$$

This key result shows that to obtain the boundary condition at $x = 0$ for the QSS PDE for $\alpha(x,t)$ we can simply substitute the outer approximation $p_1 = p_1^0(\alpha)$, $p_2 = p_2^0(\alpha)$, and $p_3 = p_3^0(\alpha)$, into the first condition of (101c). In this sense, the QSS PDE inherits the no-flux boundary condition (101c) at $x = 0$. We remark that a similar analysis can be done near $x = 1$, with the analogous result that

$$D\frac{\mathrm{d}p_3^0}{\mathrm{d}x} - v_1 p_1^0 + v_2 p_2^0 = 0, \quad \text{at} \quad x = 1. \tag{108b}$$

To complete the boundary layer analysis near $x = 0$, we expand

$$p_3 = p_{30}^0 + \frac{\varepsilon}{D}\mathscr{P}_3 + \cdots, \tag{109}$$

and obtain from the first two equations in (106), together with (107) with $A = 0$, the following boundary layer problem on $0 < \eta < \infty$:

$$v_1 p_{1\eta} = f_1\left(p_1, p_2, p_{30}^0\right); \qquad p_1(0) = 0, \quad p_1 \to p_{10}^0 \quad \text{as} \quad \eta \to \infty, \tag{110a}$$

$$v_2 p_{1\eta} = -f_2\left(p_1, p_2, p_{30}^0\right); \qquad p_2 \to p_{20}^0 \quad \text{as} \quad \eta \to \infty, \tag{110b}$$

$$\mathscr{P}_{3\eta} = v_1 p_1 - v_2 p_2; \qquad \mathscr{P}_{3\eta} \sim D\frac{dp_3^0}{dx}\Big|_{x=0} \quad \text{as} \quad \eta \to \infty. \tag{110c}$$

Although the first two equations for p_1 and p_2 are uncoupled from $\mathscr{P}_3$, in general it is not possible to calculate p_1 and p_2 analytically, especially when f_1 and f_2 are nonlinear in p_1 and p_2. However, the system for p_1 and p_2 are readily studied in the phase-plane.

We remark that a similar boundary layer analysis can be done near $x = 1$. To study this boundary layer, we now define $\eta = (1 - x)/\varepsilon$. We readily find in place of (110a) and (110b) that

$$v_1 p_{1\eta} = -f_1\left(p_1, p_2, p_{31}^0\right); \qquad p_1 \to p_{11}^0 \quad \text{as} \quad \eta \to \infty, \tag{111a}$$

$$v_2 p_{1\eta} = f_2\left(p_1, p_2, p_{30}^0\right); \qquad p_2(0) = 0, \qquad p_2 \to p_{21}^0 \quad \text{as} \quad \eta \to \infty, . \tag{111b}$$

Here $p_{j1}^0 \equiv p_j^0(\alpha(1, t))$, for $j = 1, \ldots, 3$.

D.1 The Kinesin Model

For the kinesin model (25) of Sect. 4.1, the boundary layer system (110) can be solved explicitly. With the QSS approximation $\mathbf{p}^0$, as given in (27), we identify $v_1 = v_2 = 1$, $p_1 = p^{\mathrm{R}}$, $p_2 = p^{\mathrm{L}}$, and $p_3 = p^{\mathrm{U}}$. From (27), we calculate that $p_{10}^0 = k_{\mathrm{a}} P(0) g(\alpha_0)$, $p_{20}^0 = k_{\mathrm{a}}\left[1 - P(0)\right] g(\alpha_0)$, and $p_{30}^0 = \alpha(0)$, where $\alpha_0 \equiv \alpha(0, t)$. Therefore, using the reaction kinetics in (25), (110) becomes

$$p_{1\eta} = p_{10}^0 - p_1, \qquad p_{2\eta} = -p_{20}^0 + p_2, \qquad \mathscr{P}_{3\eta} = p_1 - p_2. \tag{112}$$

The solution with $p_1(0) = 0$ and $p_2 \to p_{20}^0$ as $\eta \to \infty$, is simply $p_1 = p_{10}^0(1 - e^{-\eta})$, and $p_2 = p_{20}^0$. Then, $\mathscr{P}_3$ is obtained up to a constant by integrating the last equation in (112). In this way, we obtain the boundary layer solution for $x = \mathscr{O}(\varepsilon)$ that

$$\begin{aligned} p^{\mathrm{R}} &\sim p_{10}^0\left(1 - e^{-x/\varepsilon}\right), \qquad p^{\mathrm{L}} \sim p_{20}^0, \\ p^{\mathrm{U}} &= p_{30}^0 + \frac{\varepsilon}{D}\left(\eta D\frac{\mathrm{d}\alpha}{\mathrm{d}x}\Big|_{x=0} + p_{10}^0 e^{-\eta} + A_3\right), \end{aligned} \tag{113}$$

where the constant A_3 can only be determined from a two-term outer QSS solution, which is intractable analytically. This analysis shows two key features. Firstly, the right-moving motors have a classic boundary layer behaviour when $x = \mathcal{O}(\varepsilon)$. Secondly, for $x = \mathcal{O}(\varepsilon)$ the unbound kinesin motor density p^{U} differs from its outer approximation only by an error $\mathcal{O}(\varepsilon/D)$. A similar calculation can be done for the boundary layer near $x = 1$ using (111). We leave the details to the reader.

D.2 The Kinesin–Dynein Model

For the kinesin–dynein model (49), the boundary layer equations (110) for the layer near $x = 0$ is analysed via the phase-plane. Using $\mathbf{f}$ in (49), and setting $v_1 = 1$ and $v_2 = v$, (110a) and (110b) on $0 < \eta < \infty$ become

$$\begin{aligned} &p_{1\eta} = -p_1 - k p_1 p_2 + k_{\mathrm{a}} Q p_{30}^0, \qquad p_1(0) = 0, \\ &p_1 \to p_{10}^0 \equiv \frac{Q\alpha_0}{k\alpha_0 + 1 - Q} \quad \text{as} \quad \eta \to +\infty, \end{aligned} \tag{114a}$$

$$p_{2\eta} = -\frac{1}{v}\left[k_{\mathrm{a}}(1-Q)p_{30}^0 - p_2 + k p_1 p_2\right], \qquad p_2 \to \alpha_0 \quad \text{as} \quad \eta \to +\infty, \tag{114b}$$

where $p_{30}^0 = (k\alpha_0 + 1)\alpha_0/[k_a(k\alpha_0 + 1 - Q)]$. To analyse (114) in the phase-plane, it is convenient to introduce new variables $q_1(\eta)$ and $q_2(\eta)$ defined by

$$p_1 = \frac{r_2}{k} q_1, \qquad p_2 = \frac{r_1}{k} q_2, \qquad \text{where} \qquad r_1 = k\alpha_0, \qquad r_2 \equiv \frac{Q r_1}{r_1 + 1 - Q}. \tag{115}$$

In terms of q_1 and q_2, (114) transforms to the two-component dynamical system

$$\begin{aligned} &q_{1\eta} = g_1(q_1, q_2) \equiv (1 - q_1) + r_1(1 - q_1 q_2), \qquad q_1(0) = 0, \\ &q_1 \to 1 \quad \text{as} \quad \eta \to +\infty, \end{aligned} \tag{116a}$$

$$q_{2\eta} = g_2(q_1, q_2) \equiv -\frac{1}{v}\left[1 - q_2 + r_2(q_1 q_2 - 1)\right], \qquad q_2 \to 1 \quad \text{as} \quad \eta \to +\infty. \tag{116b}$$

As a function of r_1, we have $r_2 = 0$ when $r_1 = 0$, $r_2 \to Q < 1$ as $r_1 \to \infty$, and that r_2 is monotone increasing in r_1 since $dr_2/dr_1 = [Q(1-Q)]/(r_1 + 1 - Q)^2 > 0$ holds for $0 < Q < 1$. It follows that $0 < r_2 < 1$ for any $r_1 > 0$.

By calculating the Jacobian J_g of g_1 and g_2 at the equilibrium state $q_1 = q_2 = 1$, we find that

$$\det(J_g) = -\frac{1}{v\,(k\alpha_0 + 1 - Q)}\left[(1-Q)(1 + 2k\alpha_0) + k\alpha_0^2\right] < 0,$$

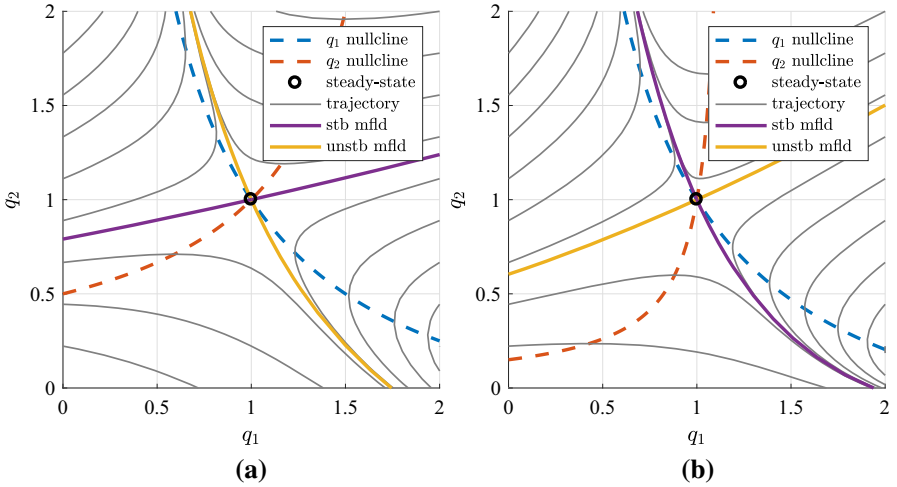

Fig. 18 Qualitative analysis of boundary layer behaviour of the kinesin–dynein model. Phase portraits of q_2 versus q_1 for boundary layer solutions of the kinesin–dynein model near $x = 0$ (**a**) and near $x = 1$ (**b**) from (116) and (117), respectively. In **a** there is a unique value $q_2 = q_2^0$ at $q_1 = 0$ for which (116) has a solution with $(q_1, q_2) \to (1, 1)$ as $\eta \to +\infty$. In **b** there is a unique value $q_1 = q_1^0$ at $q_2 = 0$ for which (117) has a solution with $(q_1, q_2) \to (1, 1)$ as $\eta \to +\infty$. The parameter values of r_1, r_2, and v for **b** are those consistent with Fig. 7. **a** $r_1 = 2.0$, $r_2 = 0.5$, $v = 0.5$. **b** $r_1 = 1.69$, $r_2 = 0.85$, $v = 0.5$ (Color figure online)

so that $q_1 = q_2 = 1$ is a saddle point for the dynamics. In Fig. 18a we plot the phase portrait q_2 versus q_1 and nullclines for (116) for representative values $r_1 = 2$, $r_2 = 0.5$, and $v = 0.5$. We observe that the q_2 nullcline intersects the q_2 axis at $q_2 = 1 - r_2 \in (0, 1)$ since $0 < r_2 < 1$. This plot indicates the existence of a unique value $q_2(0) = q_2^0 > 1 - r_2$ for which (116) has a solution with $(q_1, q_2) \to (1, 1)$ as $\eta \to +\infty$. This qualitative analysis confirms the existence of a boundary layer solution near $x = 0$ for the kinesin–dynein model for all range of parameters.

A similar phase-plane analysis can be performed to analyse the boundary layer system (111) near $x = 1$. In place of (116), we obtain that

$$q_{1\eta} = -g_1(q_1, q_2) \equiv -\left[(1 - q_1) + r_1(1 - q_1 q_2)\right], \qquad q_1 \to 1 \quad \text{as} \quad \eta \to +\infty, \tag{117a}$$

$$q_{2\eta} = -g_2(q_1, q_2) \equiv \frac{1}{v}\left[1 - q_2 + r_2(q_1 q_2 - 1)\right], \qquad q_2(0) = 0$$
$$q_2 \to 1 \quad \text{as} \quad \eta \to +\infty, \tag{117b}$$

where in place of (115), r_1 and r_2 are now defined by $r_1 = k\alpha_1$ and $r_2 \equiv Qr_1/(r_1 + 1 - Q)$, where $\alpha_1 = \alpha$ at $x = 1$. In Fig. 18b we plot the phase portrait and nullclines for (117) for $r_1 = 1.69$, $r_2 = 0.85$, and $v = 0.5$, which corresponds to the parameter values used in the caption of Fig. 7. This phase portrait shows the existence of a unique value $q_1(0) = q_1^0$ for which (117) has a solution with $(q_1, q_2) \to (1, 1)$ as $\eta \to +\infty$. Our computations yield $q_1^0 \approx 1.95$, so that from (115) we get $p_1 \approx 0.83$ at $x = 1$.

D.3 The Myosin Model

For the full myosin transport model (90), the boundary layer equations (110a)–(110b) near $x = 0$ can be studied qualitatively in the phase-plane. Upon setting $v_1 = 1$ and $v_2 = v$, (110a) and (110b) on $0 < \eta < \infty$ become

$$p_{1\eta} = -k_{\rm bw} p_1 p_2^2 - p_1 + k_{\rm b} p_{30}^0, \qquad p_1(0) = 0,$$
$$p_1 \to p_{10}^0 \equiv \frac{1}{k_{\rm bw}\alpha_0}, \quad \text{as} \quad \eta \to +\infty, \tag{118a}$$

$$p_{2\eta} = -\frac{1}{v}\left(k_{\rm bw} p_1 p_2^2 - p_2\right), \qquad p_2 \to \alpha_0 \quad \text{as} \quad \eta \to +\infty, \tag{118b}$$

where $p_{30}^0 = (\alpha_0 + 1/[k_{\rm bw}\alpha_0])/k_{\rm b}$ and $\alpha_0 = \alpha(0, t)$. We conveniently introduce new variables q_1 and q_2 defined by

$$p_1 = \frac{1}{k_{\rm bw}\alpha_0} q_1, \qquad p_2 = \alpha_0 q_2, \tag{119}$$

so that in terms of $r \equiv k_{\rm bw}\alpha_0^2$, (118) becomes

$$q_{1\eta} = g_1(q_1, q_2)$$
$$\equiv -r\left(q_1 q_2^2 - 1\right) + 1 - q_1, \qquad q_1(0) = 0, \qquad q_1 \to 1 \quad \text{as} \quad \eta \to +\infty, \tag{120a}$$

$$q_{2\eta} = g_2(q_1, q_2) \equiv -\frac{1}{v}\left(q_1 q_2^2 - q_2\right), \qquad q_2 \to 1 \quad \text{as} \quad \eta \to +\infty. \tag{120b}$$

At the equilibrium state $q_1 = q_2 = 1$, the determinant of the Jacobian J_g of g_1 and g_2 is $\det(J_g) = (1 - r)/v$. Therefore, $\det(J_g) < 0$ and $q_1 = q_2 = 1$ is a saddle point if $r \equiv k_{\rm bw}\alpha_0^2 > 1$. In Fig. 19a we plot the phase portrait of q_2 versus q_1 and nullclines for (120) for the representative values $r = 5$ and $v = 0.5$. We observe that there is a unique value $q_2(0) = q_2^0$ for which (120) has a solution with $(q_1, q_2) \to (1, 1)$ as $\eta \to +\infty$. As such, there is always a boundary layer solution near $x = 0$ for the myosin model.

A similar boundary layer system near $x = 1$ can be obtained from (111) for the myosin model. In place of (120), we obtain that

$$q_{1\eta} = -g_1(q_1, q_2) \equiv r\left(q_1 q_2^2 - 1\right) - 1 + q_1, \qquad q_1 \to 1 \quad \text{as} \quad \eta \to +\infty, \tag{121a}$$

$$q_{2\eta} = -g_2(q_1, q_2) \equiv \frac{1}{v}\left(q_1 q_2^2 - q_2\right), \qquad q_2(0) = 0 \qquad q_2 \to 1 \quad \text{as} \quad \eta \to +\infty, \tag{121b}$$

where r is now defined by $r = k_{\rm bw}\alpha_1^2$ with $\alpha_1 = \alpha(1, t)$. Although the equilibrium point $q_1 = q_2 = 1$ is a saddle point of (121) whenever $r > 1$, the phase portrait in the

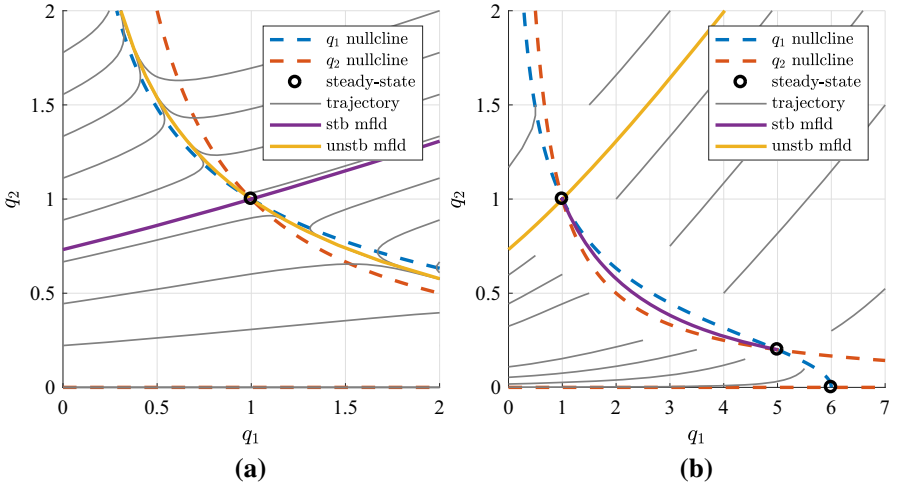

Fig. 19 Qualitative analysis of boundary layer behaviour of the myosin model. Phase portraits of q_2 versus q_1 for boundary layer solutions of the myosin model near $x = 0$ (**a**) and near $x = 1$ (**b**) from (120) and (121), respectively. In **a** there is a unique value $q_2 = q_2^0$ at $q_1 = 0$ for which (120) has a solution with $(q_1, q_2) \to (1, 1)$ as $\eta \to +\infty$. However, for the right boundary layer, the phase-plane in **b** there is no value $q_1 = q_1^0 > 0$ at $q_2 = 0$ for which $(q_1, q_2) \to (1, 1)$ as $\eta \to \infty$. **a** $r = 5$, $v = 0.5$. **b** $r = 5$, $v = 0.5$ (Color figure online)

q_2 versus q_1 plane shown in Fig. 19b shows that there is **no value** $q_1(0) = q_1^0 > 0$ on $q_2 = 0$ for which $(q_1, q_2) \to (1, 1)$ as $\eta \to \infty$.

As such, we conclude for the Type II QSS approximation (64) for the myosin model that there is no steady-state boundary layer solution near $x = 1$ that allows the extra boundary condition $p^{\mathrm{B}} = 0$ at $x = 1$ to be satisfied.

References

Baas PW, Deitch JS, Black MM, Banker GA (1988) Polarity orientation of microtubules in hippocampal neurons: uniformity in the axon and nonuniformity in the dendrite. Proc Natl Acad Sci 85(21):8335–8339

Bhat D, Gopalakrishnan M (2012) Effectiveness of a dynein team in a tug of war helped by reduced load sensitivity of detachment: evidence from the study of bidirectional endosome transport in D. discoideum. Phys Biol 9(4):46003

Blasius TL, Reed N, Slepchenko BM, Verhey KJ (2013) Recycling of kinesin-1 motors by diffusion after transport. PLoS One 8(9):e76081

Bressloff P, Newby J (2013) Stochastic models of intracellular transport. Rev Mod Phys 85(1):135–196

Bressloff PC, Newby JM (2011) Quasi-steady-state analysis of two-dimensional random intermittent search processes. Phys Rev E 83(6):061139

Burton PR (1988) Dendrites of mitral cell neurons contain microtubules of opposite polarity. Brain Res 473(1):107–115

Chowdhury D, Schadschneider A, Nishinari K (2005) Traffic phenomena in biology: from molecular motors to organisms. Traffic Granul Flow 2(4):223–238

Ciandrini L, Romano MC, Parmeggiani A (2014) Stepping and crowding of molecular motors: statistical kinetics from an exclusion process perspective. Biophys J 107(5):1176–1184

Dauvergne D, Edelstein-Keshet L (2015) Application of quasi-steady state methods to molecular motor transport on microtubules in fungal hyphae. J Theor Biol 379:47–58
Dixit R, Ross JL, Goldman YE, Holzbaur ELF (2008) Differential regulation of dynein. Science 319(February):8–11
Fink G, Steinberg G (2006) Dynein-dependent motility of microtubules and nucleation sites supports polarization of the tubulin array in the fungus Ustilago maydis. Mol Biol Cell 17(7):3242–3253
Gou J, Edelstein-Keshet L, Allard J (2014) Mathematical model with spatially uniform regulation explains long-range bidirectional transport of early endosomes in fungal hyphae. Mol Biol Cell 25(16):2408–2415
Hendricks AG, Perlson E, Ross JL, Schroeder HW, Tokito M, Holzbaur ELF (2010) Motor coordination via a tug-of-war mechanism drives bidirectional vesicle transport. Curr Biol 20(8):697–702
Klumpp S, Lipowsky R (2005) Cooperative cargo transport by several molecular motors. Proc Natl Acad Sci USA 102(48):17284–17289
Leduc C, Padberg-Gehle K, Varga V, Helbing D, Diez S, Howard J (2012) Molecular crowding creates traffic jams of kinesin motors on microtubules. Proc Natl Acad Sci USA 109(16):6100–6105
Mallik R, Rai AK, Barak P, Rai A, Kunwar A (2013) Teamwork in microtubule motors. Trends Cell Biol 23(11):575–582
Mattila PK, Lappalainen P (2008) Filopodia: molecular architecture and cellular functions. Nat Rev Mol Cell Biol 9(6):446–454
McVicker DP, Chrin LR, Berger CL (2011) The nucleotide-binding state of microtubules modulates kinesin processivity and the ability of Tau to inhibit kinesin-mediated transport. J Biol Chem 286(50):42873–42880
Müller MJI, Klumpp S, Lipowsky R (2008) Motility states of molecular motors engaged in a stochastic tug-of-war. J Stat Phys 133(6):1059–1081
Nambiar R, McConnell RE, Tyska MJ (2010) Myosin motor function: the ins and outs of actin-based membrane protrusions. Cell Mol Life Sci 67(8):1239–1254
Newby J, Bressloff PC (2010a) Local synaptic signaling enhances the stochastic transport of motor-driven cargo in neurons. Phys Biol 7(3):036004
Newby JM, Bressloff PC (2010b) Quasi-steady state reduction of molecular motor-based models of directed intermittent search. Bull Math Biol 72(7):1840–1866
Parmeggiani A, Franosch T, Frey E (2004) Totally asymmetric simple exclusion process with langmuir kinetics. Phys Rev E 70(4):046101
Reed NA, Cai D, Blasius TL, Jih GT, Meyhofer E, Gaertig J, Verhey KJ (2006) Microtubule acetylation promotes kinesin-1 binding and transport. Curr Biol 16(21):2166–2172
Reichenbach T, Frey E, Franosch T (2007) Traffic jams induced by rare switching events in two-lane transport. New J Phys 9(6):159
Rzadzinska AK, Schneider ME, Davies C, Riordan GP, Kachar B (2004) Stereocilia functional architecture and self-renewal. J Cell Biol 164(6):887–897
Schneider ME, Dose AC, Salles FT, Chang W, Erickson FL, Burnside B, Kachar B (2006) A new compartment at stereocilia tips defined by spatial and temporal patterns of myosin IIIa expression. J Neurosci 26(40):10243–10252
Schuster M, Kilaru S, Fink G, Collemare J, Roger Y, Steinberg G (2011a) Kinesin-3 and dynein cooperate in long-range retrograde endosome motility along a nonuniform microtubule array. Mol Biol Cell 22(19):3645–3657
Schuster M, Lipowsky R, Assmann M-A, Lenz P, Steinberg G (2011b) Transient binding of dynein controls bidirectional long-range motility of early endosomes. Proc Natl Acad Sci USA 108(9):3618–3623
Schwander M, Kachar B, Müller U (2010) Review series: the cell biology of hearing. J. Cell Biol 190(1):9–20
Shubeita GT (2012) Intracellular transport: relating single-molecule properties to in vivo function. Compr Biophys 4:287–297
Smith DA, Simmons RM (2001) Models of motor-assisted transport of intracellular particles. Biophys J 80(1):45–68
Steinberg G (2011) Motors in fungal morphogenesis: cooperation versus competition. Curr Opin Microbiol 14(6):660–667
Steinberg G, Wedlich-Soldner R, Brill M, Schulz I (2001) Microtubules in the fungal pathogen Ustilago maydis are highly dynamic and determine cell polarity. J Cell Sci 114(Pt 3):609–622
Stone MC, Roegiers F, Rolls MM (2008) Microtubules have opposite orientation in axons and dendrites of drosophila neurons. Mol Biol Cell 19(10):4122–4129

Yochelis A, Gov NS (2016) Reaction–diffusion–advection approach to propagating aggregates of molecular motors. Phys D 318–319:1–15

Yochelis A, Ebrahim S, Millis B, Cui R, Kachar B, Naoz M, Gov NS (2015) Self-organization of waves and pulse trains by molecular motors in cellular protrusions. Sci Rep 5:13521